JPL NO. 9950-287

DRD Line No. SE-6

DOE/JPL-955164 79/4
Distribution Category UC-63

DEVELOPMENT OF ECONOMICAL IMPROVED THICK FILM SOLAR CELL CONTACT

BERND ROSS

BERND ROSS ASSOCIATES
2154 Blackmore Court
San Diego, CA 92109

EXTENSION FINAL REPORT
April 1979 - Dec. 1979

December 1979

Contractual Acknowledgement

The JPL Low-Cost Silicon Solar Array Project is sponsored by the U. S. Department of Energy and forms part of the Solar Photovoltaic Conversion Program to initiate a major effort toward the development of low-cost solar arrays. This work was performed for the Jet Propulsion Laboratory, California Institute of Technology by agreement between NASA and DOE.

DRD Line No. SE-6

DOE/JPL-955164 79/4
Distribution Category UC-63

DEVELOPMENT OF ECONOMICAL IMPROVED THICK FILM SOLAR CELL CONTACT

BERND ROSS

BERND ROSS ASSOCIATES
2154 Blackmore Court
San Diego, CA 92109

EXTENSION FINAL REPORT
April 1979 - Dec. 1979

December 1979

Contractual Acknowledgement

The JPL Low-Cost Silicon Solar Array Project is sponsored by the U. S. Department of Energy and forms part of the Solar Photovoltaic Conversion Program to initiate a major effort toward the development of low-cost solar arrays. This work was performed for the Jet Propulsion Laboratory, California Institute of Technology by agreement between NASA and DOE.

TABLE OF CONTENTS

TABLE OF CONTENTS Cont.

TABLE OF FIGURES

TABLE OF FIGURES Cont.

TABLE OF FIGURES Cont.

LIST OF TABLES

1.0 SUMMARY

In the second half of the investigation of all metal screened electrodes, the focus was on base metal pastes in addition to further work with the silver systems. Contact resistance measurements were refined. A facility allowing firing in hydrogen and other atmospheres was acquired. Several experiments were made applying screenable pastes to solar cells. Doping investigations emphasized eutectic alloys reduced to powders. Metal systems were reviewed. A previously published vapor pressure curve for silver fluoride was corrected. Base metal experiments were done with nickel and copper using lead and tin as the frit metals. Severe adhesion problems were experienced with hydrogen atmospheres in all metal systems. A two step firing schedule was devised based upon experimentation which gave evidence that the silver fluoride-silicon dioxide reaction was modified by the presence of hydrogen. It was found that nitrogen prefiring allowed the silver fluoride dissociation and oxide removal without causing catastrophic oxidation of the base metal powders. The subsequent hydrogen firing step reduced oxides that had formed and gave the proper sintered structure. Electrodes were coherent, adherent, and solderable in both nickel lead and copper lead systems. Towards the end of the contractual period aluminum-silicon and aluminum-germanium eutectic doping additions to copper pastes were tried on 2 1/4" diameter solar cell back contacts, both with good results (η = 9.4% AM1 uncoated).

No electrical experiments were done with the nickel ink. Problems were experienced with a digital voltmeter causing delay in the contact resistance measurements. A new instrument was acquired. Furnace elements were repaired after burnout, a flow valve was replaced in the gas handling system, and a modification was made on the furnace to accommodate a longer quartz tube to reduce oxidation. A serious calibration error was found in the control thermocouple of the firing facility. Calibration standards and associated electronics were acquired to prevent recurrence of this problem.

2.0 INTRODUCTION

The potential for economy and efficiency has been demonstrated for the thick film metallization process using screen printing for solar cell electrodes. However, process reliability and materials economy remain deficient. It is believed that these deficiencies can be removed by the use of ink formulations designed specifically for silicon solar cells, departing from ceramic technology tradition and utilizing all metal systems. The objectives of this investigation are as follows:

1. Eliminate the glass frit which has been the conventional liquid phase sintering medium and adhesive for metallization inks.

2. Provide an appropriate metal which can serve as the liquid phase sintering medium.

3. Find a chemical constituent which effectively removes the native oxide from the silicon during the firing step, which can be made part of the ink, and which either becomes fugitive or remains an inert part of the matured metallization.

4. Maintain cognizance of the cost objectives of the LSA Project in selecting materials and processes.

3.0 SERIES RESISTANCE AND CONTACT RESISTANCE CONSIDERATIONS

The measurement of contact resistance has been problematical since the work with thick film electrodes began. Several methods have been utilized in the past using either silicon material or solar cells as a point of departure. A relatively simple method uses a silicon rod of simple shape shown in Figure 1. The resistivity of the rod is determined by other means (such as a four point probe). The resistance of the rod and contacts is measured across the two electrodes. The contact resistance is

$$R_C = R - \rho \frac{L}{A}$$

where R = total resistance in Ω

ρ = resistivity of the silicon material in Ωcm

L = length of rod in cm

A = area of contact in cm^2

While the method has the virtue of analytical simplicity, it is experimentally somewhat cumbersome and requires resistivity determination prior to attaching contacts, with no guarantee that the resistivity remains unchanged as a function of the firing process. In our measurements the series resistance between two adjacent squares of a screened standard pattern was used. The actual current flux pattern in such a configuration is complex and can be handled by using the formalism of source and sink images[1]. For our purposes an average current path was estimated, the resistivity of the wafers was in a fairly tight group and only relative measure-

ments were required. Nevertheless, the variation in results and reproducibility problems caused us to lose confidence in the method.

In dealing with diodes or solar cells, contact resistance is a part of the series resistance, including IR drops of semiconductor regions and electrode regions themselves. While some of these can be measured with difficulty, assumptions as to their magnitude are usually made. The series resistance can then be determined from an extended IV curve (log I versus V) by noting the departure from the exponential diode characteristic[2]. Another method utilizes multiple light levels with series resistance measured by taking incremental currents and noting the shift in corresponding terminal voltage[3]. (See Figure 2). None of the above methods were considered optimal for this investigation. Therefore, a literature study was undertaken to find a better method.

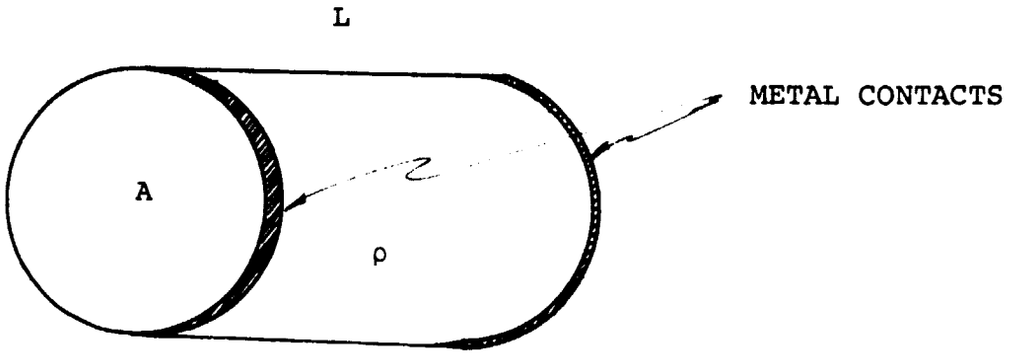

Fig. 1. Simple Resistance - Contact Resistance Measurement

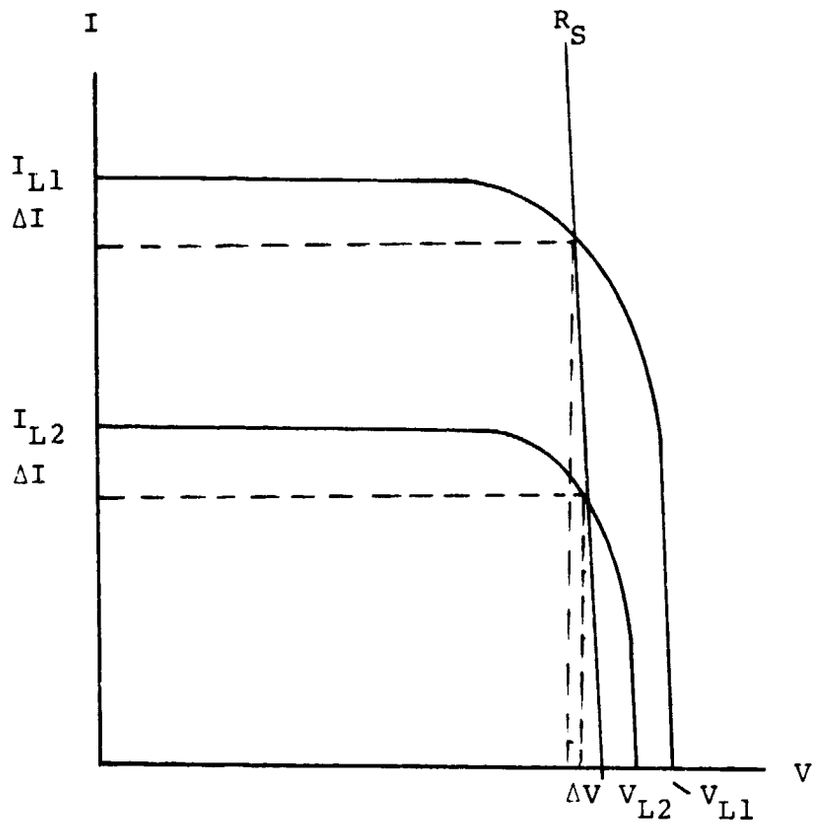

Fig. 2. Series Resistance Measurement by Illumination Level Change (L. D. Swanson's Method)

3.1 Contact Resistance Measurement Method

A reference was found to a contact resistance measurement proposed by W. Shockley. The method was designed to accommodate field effect transistors and was described by Hower et al[4]. The measurement scheme is well-suited to contact resistance evaluation of electrodes or electrode arrays on solar cell material prior to cell processing, pn-junction formation, etc. Since the existence of a conducting sheet on the opposite side of the wafer would severely alter the current flux densities and contours, the test would be less suitable for completed solar cells. While the dimensions of the semiconductor layer and electrodes are quite different in the case of the solar cell experiments from the original FET designs, there are no fundamental reasons why the measurement should not work for our purposes. The method can best be illustrated by Figure 3. Figure 3 (a) shows a contact metal layer on a semiconductor wafer with dimensions x and z (with y dimension arbitrary). The schematic (b) below (a) considers the semiconductor a chain of sheet resistances $R_{\square}$ (in units of ohms per square) connected to the grounded metal contact by contact resistances R_c in ladder network fashion. Since the metal resistance is very small compared to the other resistances involved, it may be neglected in this formulation. The current I flowing through the semiconductor wafer enters the region below the metal contact at x = 0. A portion of the current, ΔI enters the electrode through R_c and diminishes the wafer current I. This

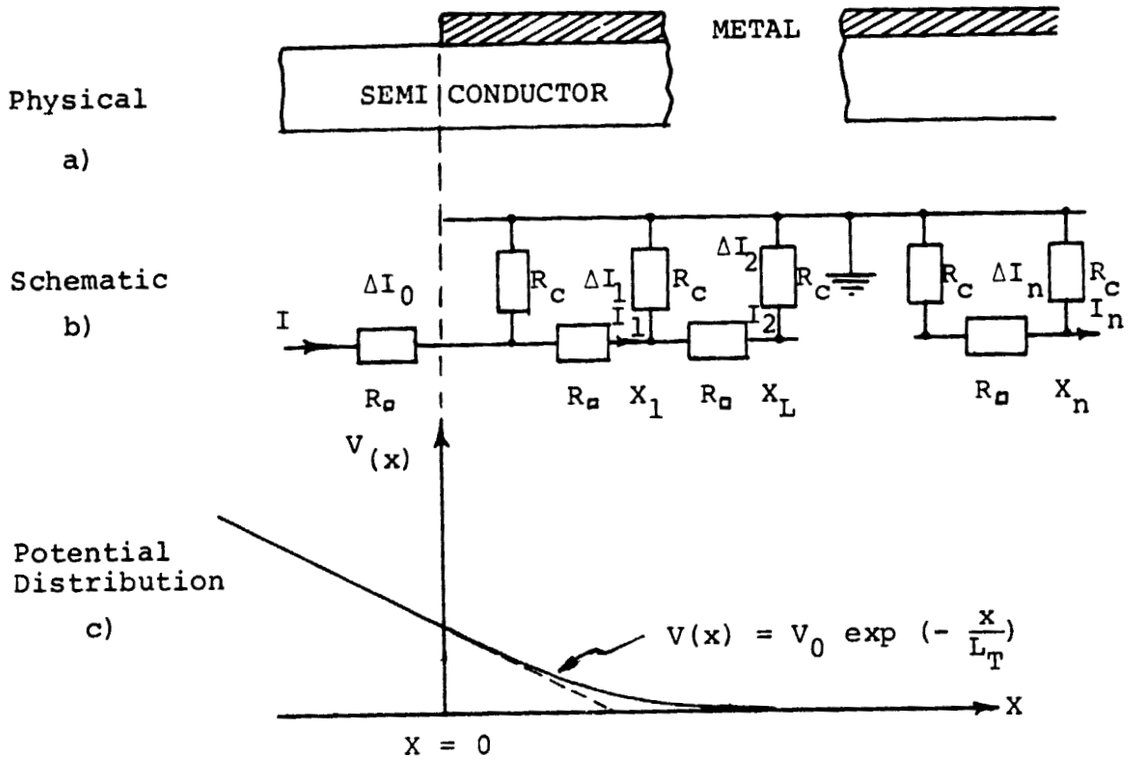

Fig. 3. Metal Semiconductor Contact

results in a potential distribution V(x) given by Figure 3(c).

The differential equation describing the stated conditions is

$$\frac{R_C}{R_\square} \frac{d^2V(x)}{dx^2} - V(x)\,dx = 0$$

with solution

$$V(x) = V_o \exp\left(- \frac{X}{L_T}\right)$$

where $L_T \equiv$ Transfer length

$$= \sqrt{R_C/R_\square}$$

All other quantities were previously defined.

3.2 Contact Resistance Measurement Results

The method was reduced to practice by designing masks shown in Figure 4. The current source and drain contacts were squares of 2.5mm edge length spaced to allow potential probe contacts to be placed at equal intervals between them. The small contacts were 0.25mm wide, 0.6mm long and placed on 0.5mm centers. Separate masks were fabricated so that current and voltage contacts could be separately screened.

Figures 5 and 6 show actual photomicrographs of the electrode patterns.

Measurements are performed as follows: A constant current source is connected between the large squares. The potential of the contact lines is probed by connecting one of the current electrodes on the LOW side of a digital voltmeter with good resolution (0.1 mV or better). The HIGH side of the voltmeter is then used to measure the potential on each line electrode. The potential measurements V(x) are then plotted as the ordinate against the dimensionless abscissa x. The transfer length is obtained by extrapolating the straight portion of V(x) beyond x=0 to V(x) = 0. Physically, the transfer length is the distance that the current must flow under the contact before 0.632I is transferred to the contact. The resistance $R_{\square}$ can be calculated from

$$R_{\square} = \frac{\Delta V(x)}{I} \frac{Z}{L}$$

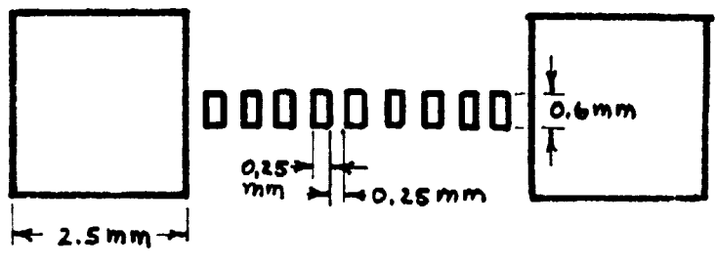

Figure 4. Masks for Contact Resistance Measurement

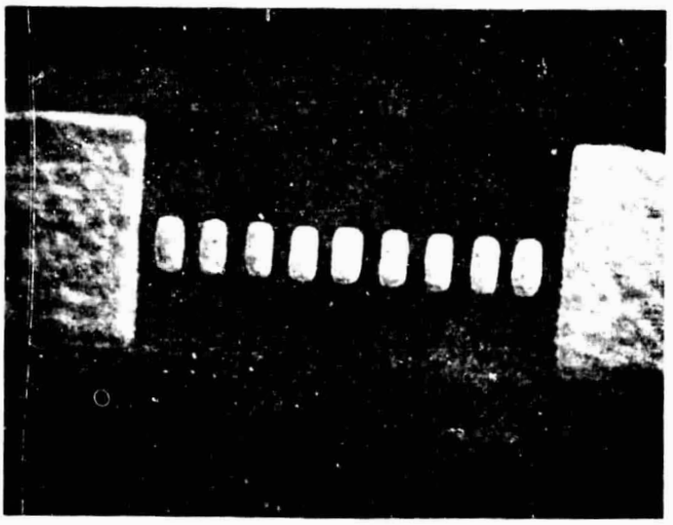

Fig. 5. S058 screened contact pattern for contact resistance measurement on polished silicon wafer prior to firing (Optical microscope magnification 13X).

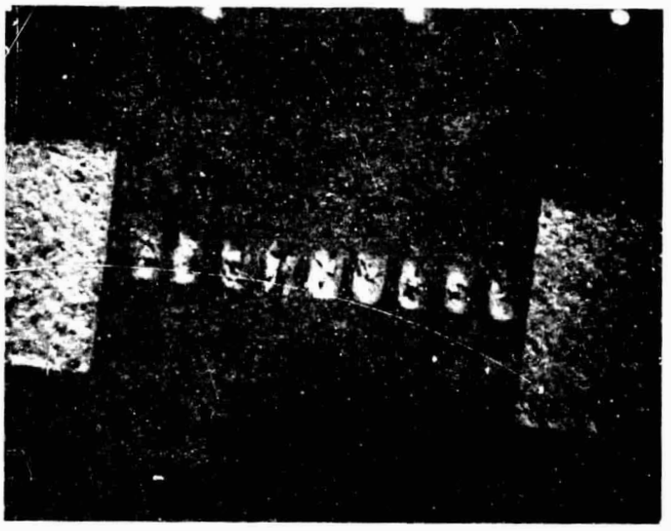

Fig. 6. S057 fired at 600°C in air screened on lapped silicon wafer. Scratches on contact pattern indicate probing from previous measurement.

where ΔV = the voltage drop along in Volts

$L \equiv$ length (in cm) of portion of the array carrying

$I \equiv$ current in amps

$Z/L \equiv$ number of squares in interval L (dimensionless)

The contact resistance R_c (in Ωcm^2) is obtained from the relation $R_c = L_T^2 R_\square$.

Initial measurements were plotted to gain familiarity with the method. The best straight line was drawn through the voltage points and the intercept on the x axis gave the transfer length L_T. Subsequently, a program was used to obtain the equation of the line using a regression coefficient to provide a measure of the degree of fit (K = 1 is the best obtainable). Data and plots for S057 fired at 550°C and 600°C in nitrogen are given in the appendix. Results for S057, S058, and S059 have given values of contact resistance from the mid 10^{-4} Ωcm^2 to mid 10^{-3} Ωcm^2.

4.0 EUTECTIC POWDER DOPING

4.1 Theoretical Consideration

The requirement for low resistance ohmic contacts makes a heavily doped semiconductor surface under the contact desirable, because of the narrowing of the metal-semiconductor potential barrier as the doping concentration increases. Screened base metal contacts for solar cells are prepared at relatively low temperatures. Thermal diffusion of doping atoms during the electrode sintering process is not likely to provide the required surface properties, since thermal energies may not be adequate to penetrate surface barriers at such low temperatures.

An alternative method of providing the ohmic contact utilizes an epitaxial deposition of highly doped semiconductor layers on the clean silicon surface. This is done by heating a eutectic composition of silicon, or germanium with aluminum. Melting occurs close to the eutectic temperature minimum (Si-Al 577°C, Ge-Al 424°C). If the composition of the material is semiconductor rich (excess of Ge or Si), the excess will go into solution in the melt in accordance with the composition dictated by the liquidus line of the phase diagram of Figures 7 and 8. The semiconductor excess can be proportioned such that it is completely dissolved in the melt at the sintering temperature. As temperature decreases, the composition varies continuously as the isotherm intersection with the liquidus line. Excess semiconductor

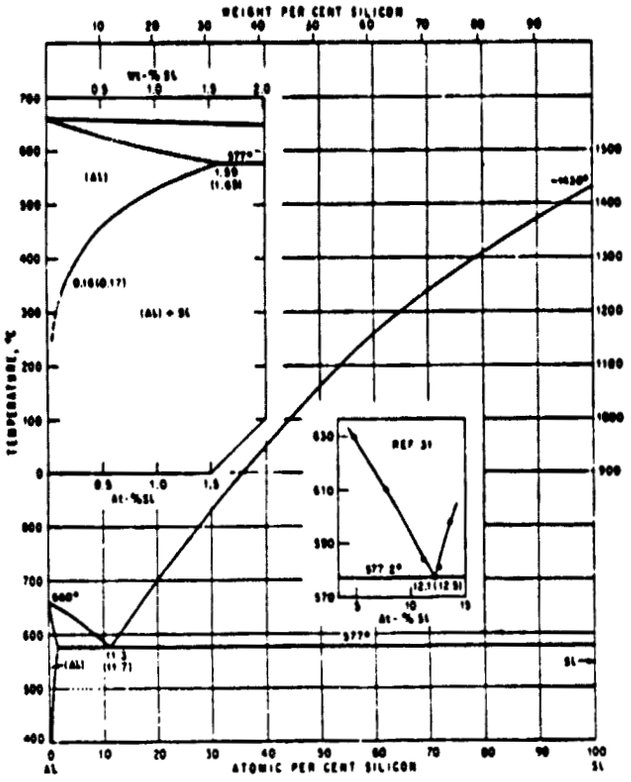

Fig. 7. Phase diagram of the aluminum-silicon system.

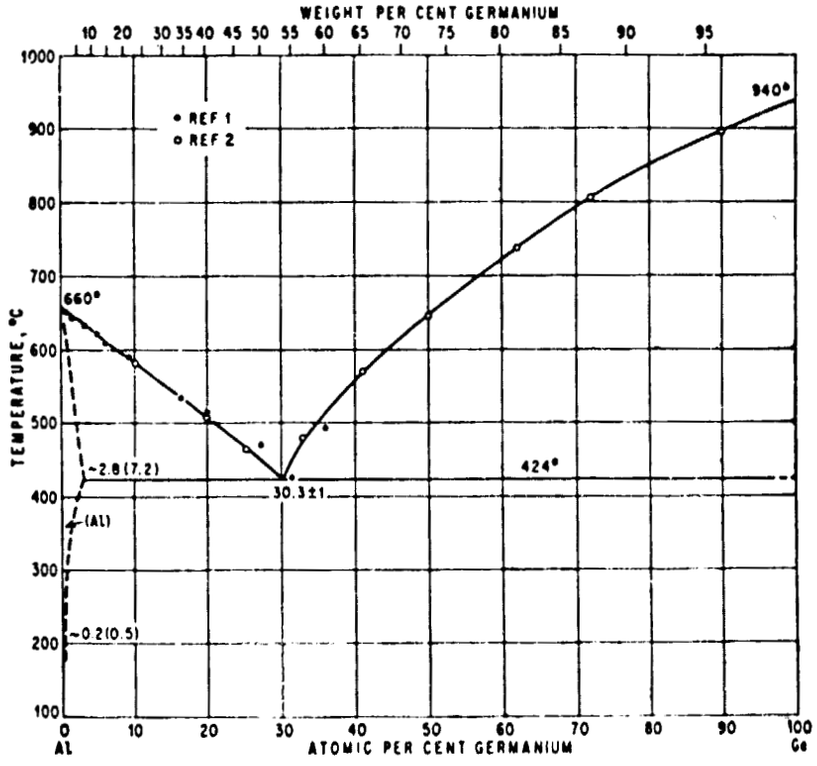

Figure 8. Phase diagram of the aluminum-germanium system

material no longer supported in solution, precipitates on convenient nucleation sites. The freshly wetted silicon surface presents such sites. The material depositing epitaxially, contains its solid solubility limit of aluminum concentration ($5 \cdot 10^{18}$ Al/cm^3).

The Schottky barrier generated by the metal-semiconductor contact has a width (t) varying as a function of the doping density (N) such that $t \propto N^{-1/2}$. The contact resistance is inversely proportional to the tunneling current which varies as exp ($-cst \cdot \phi^{1/2} t$). The barrier height (ϕ) is usually about 2/3 of the energy gap, in n-type silicon according to Spitzer and Mead[5]. Therefore the metal barrier to silicon can be taken as 0.72 eV and to germanium 0.44 eV, in n-type and 1/3 Eg in p-type giving 0.38 eV and 0.25 eV respectively.

The contact resistance of copper-silicon can be calculated to be $3 \cdot 10^{-4} \Omega cm^2$, and that of copper-germanium $2 \cdot 10^{4} \Omega cm^2$ using thermionic field emission theory with reasonable assumptions[6]. The lower resistance in the case of germanium results from the lower barrier. In addition to providing a lower contact resistance the germanium eutectic has the advantage of a lower melting point, permitting lower temperature processing.

The energy level diagram for a eutectic silicon-aluminum regrowth layer on silicon is shown in Figure 9. The metal is shown on the left side of vertical coordinate axis, the regrown silicon containing $5 \cdot 10^{18}$ Aluminum atoms per cm^3 on the right. The depletion width is 77Å and the barrier height is 0.25eV, truncated somewhat by the effect of image forces. The calculated specific contact resistance for this structure is $1.6 \cdot 10^{-4} \Omega cm^2$ at 300°C.

ENERGY LEVEL DIAGRAM

ALUMINUM ALLOY REGROWTH CONTACT

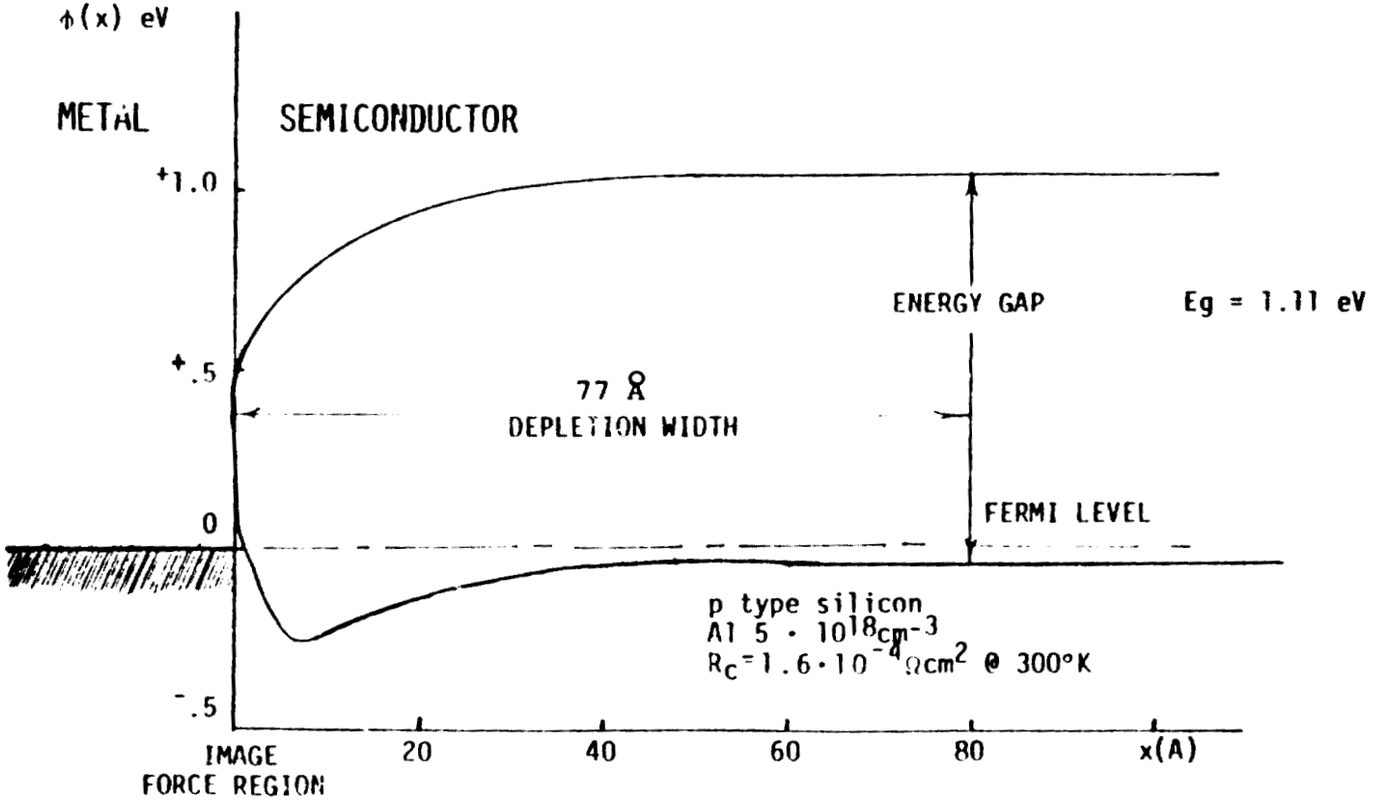

Figure 9

4.2 Powder Preparations

Aluminum-silicon and aluminum-germanium alloys were prepared by melting sizable chunks of the elements in a tube furnace with a flowing hydrogen atmosphere. The temperatures were about 200°C above the eutectic melting points, and the flow rate was 1.5 liters/min. A photograph of the eutectic alloys, as removed from the crucibles, is shown in Figure 10. Previous attempts to alloy mixed powders of the constituent metals in the same way were unsuccessful (see Figure 11). The solidified alloys, were mechanically cleaned of dark dross residues on the free surface and were reduced to -#325 mesh powders by crushing and milling. They were then combined with other constituents of all metal inks.

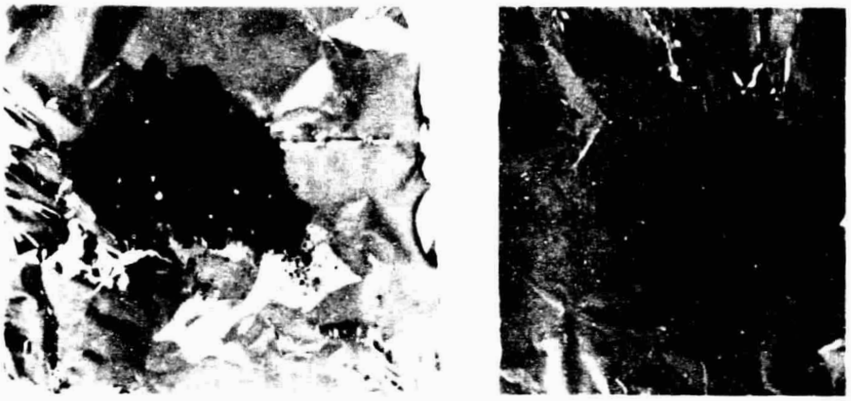

Figure 10 Aluminum-silicon (left) and aluminum-germanium (right) powders, in the eutectic ratio after firing in hydrogen, as removed from crucibles.

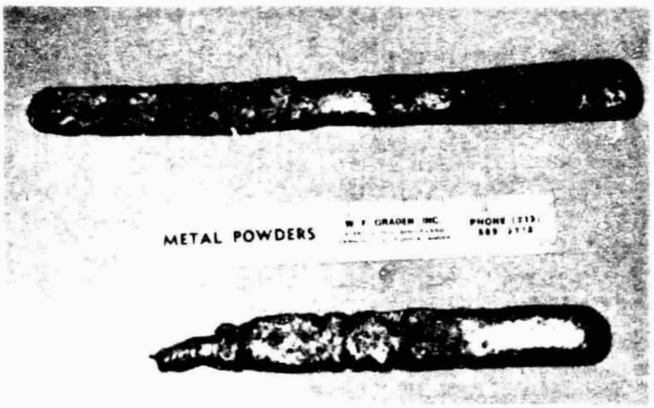

Figure 11 Aluminum-silicon (top) and aluminum-germanium (bottom) eutectic alloys, fired in hydrogen, as removed from crucibles.

4.2.1 Fabrication of Germanium-Antimony Eutectic Powder

Initial attempts to produce eutectic alloys in a nitrogen atmosphere with germanium (Ge) and aluminum (Al) as well as antimony (Sb) powders respectively, were considered unsuccessful because of excessive oxidation. The attempt was repeated using a tube furnace with a hydrogen atmosphere continuously flowing past the sample (courtesy Applied Solar Energy Corp.). The constituents were weighed (11% Ge in Sb), mixed and packed in a Pyrex ^{R} beaker. The beaker was inserted through a flame curtain into the quartz tube of the furnace and placed in a relatively cool position. The beaker remained for five minutes in the warm hydrogen stream ($\sim$0.5 $\frac{\text{liter}}{\text{min}}$) to allow purging the powder of a major portion of the entrapped air. Then the beaker was pulled into the center of the furnace which had equilibrated at 624°C and allowed to remain for 15 minutes. After insertion, the powder separated into two equal portions (vertically), with a gas space in between. After two minutes in the hot zone the gas space collapsed and densification was observed. After melting was visible, the process went to completion in two minutes. A black powder dross was found on top of the metal button. The dross was removed and the metal was found to be quite brittle and could easily be reduced to a coarse grained powder with a hammer in a plastic bag. Further reduction in grain size was easily accomplished with a mortar and pestle.

4.3 Solar Cell Experiments With Silver Inks With Eutectic Additives

A solar cell experiment was done at the premises of Applied Solar Energy Corporation with the cooperation of P.A. Iles and others. Since the antimony fraction of the inks is highly susceptible to oxidation, the ink firing operations were done in flowing hydrogen (10 minutes). Upon insertion of the cells it was noted that the screened back contact sometimes lifted and curled up. Similarly the adhesion of the front contact was very poor in some cases, coming off while maintaining identity as grid lines or collector busses.

In a previous experiment a similar result was observed with an antimony containing ink (S034). The explanation at that time was thought to be the formation of a eutectic liquid (antimony-silver), melting at 485°C with 44% antimony. It was felt that the surface tension resulting from the additional liquid might overcome the adhesion to the silicon. The quantities involved make this hypothesis weak:

Pb (liquid) 5 wt%

(Sb 0.1 wt% + Ag 0.1 wt%) (liquid).

The additional amount of liquid can only be

$$\frac{0.2\ \text{Ag}(+\ \text{Sb})}{5.0\ \text{Pb}} = .04 \text{ or } 4\ \text{wt\% of the liquid.}$$

The other ink utilized, S059, contained Ge-Al eutectic and gallium chloride.

Print fragments from the lifted electrodes were mounted and subjected to SEM examination. Figure 12 shows S034 (5% Pb, 2% AgF, 93% Ag, 0.1% Sb) at various magnifications: 200X, 1000X, 5000X and 10,000X. The appearance seems to support the above hypothesis showing a continuous sheet of metal with highly occasional pores which implies melting. This is quite different from the lacy matrix of sintered silver grains which are typical for these electrodes. At the last two magnifications the rod shaped structures can be seen which were previously identified as the precipitated lead[7].

The appearance of the other electrodes is different and Figure 13 shows portions from a print of S063 (masterpaste with germanium-antimony eutectic and probably oxides) at increasing magnifications, 510X and 5100X respectively. The color difference could be due to oxide mixtures, bearing in mind that the imaging current of the SEM derives from secondary electron yield rate, which could, in turn, be caused by charging effects. In any case the 'solid sheet' nature of the previous pictures is absent and we have a typical sintered structure. The occasional horizontal raster effect seen in Figure 14 is an artifact of the instrumentation.

The electronmicrographs from S059 (masterpaste + 5% Ge-Al eutectic + 1% gallium chloride) appear to be a combination of the previous pictures. Figure 14 shows magnification of 1000X, 5000X and 10,000X of the subject peeled electrode. The discoloration effect

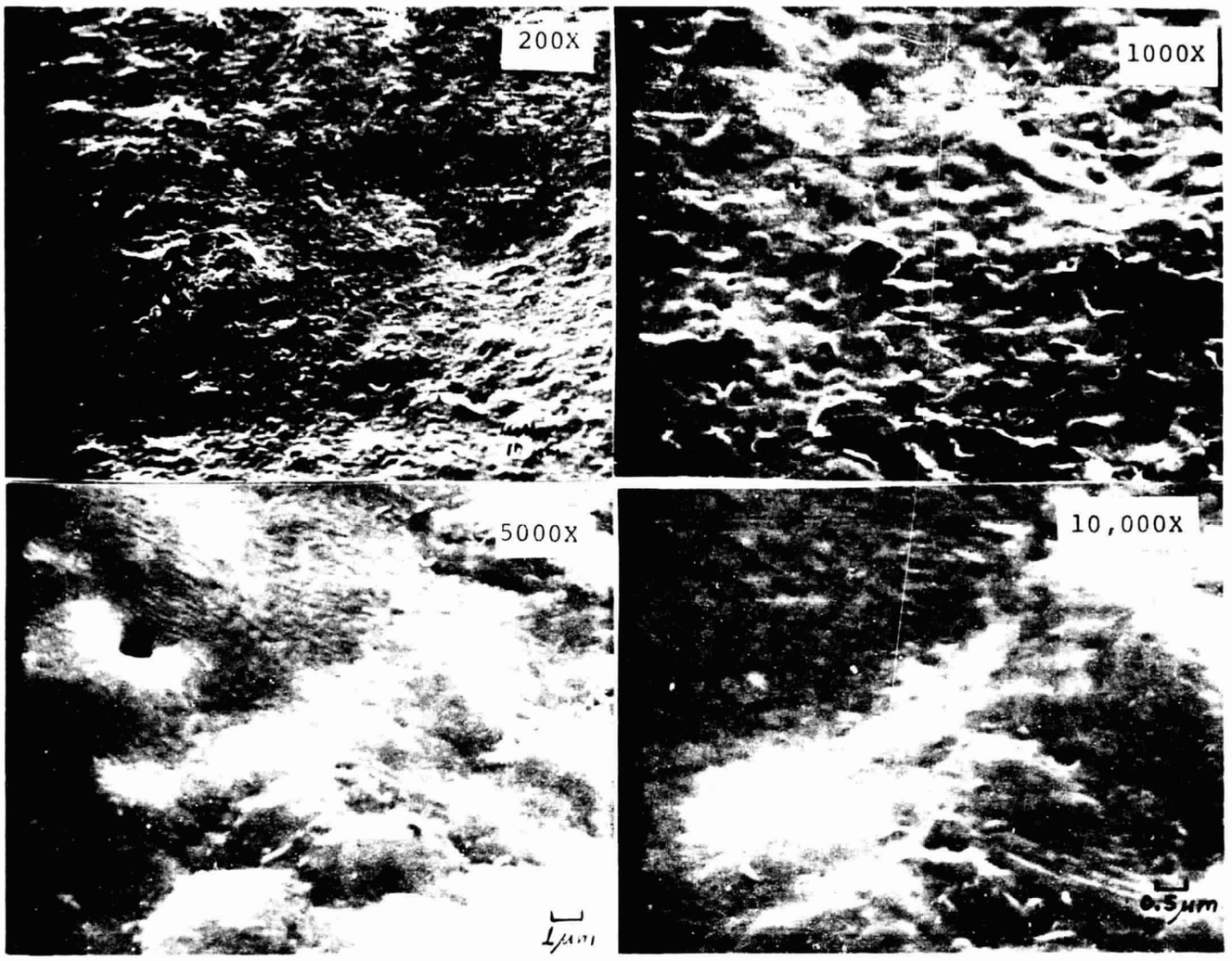

Fig. 12 Photomicrograph of peeled electrode print S034 fired in hydrogen at 650°C taken on Cambridge SEM

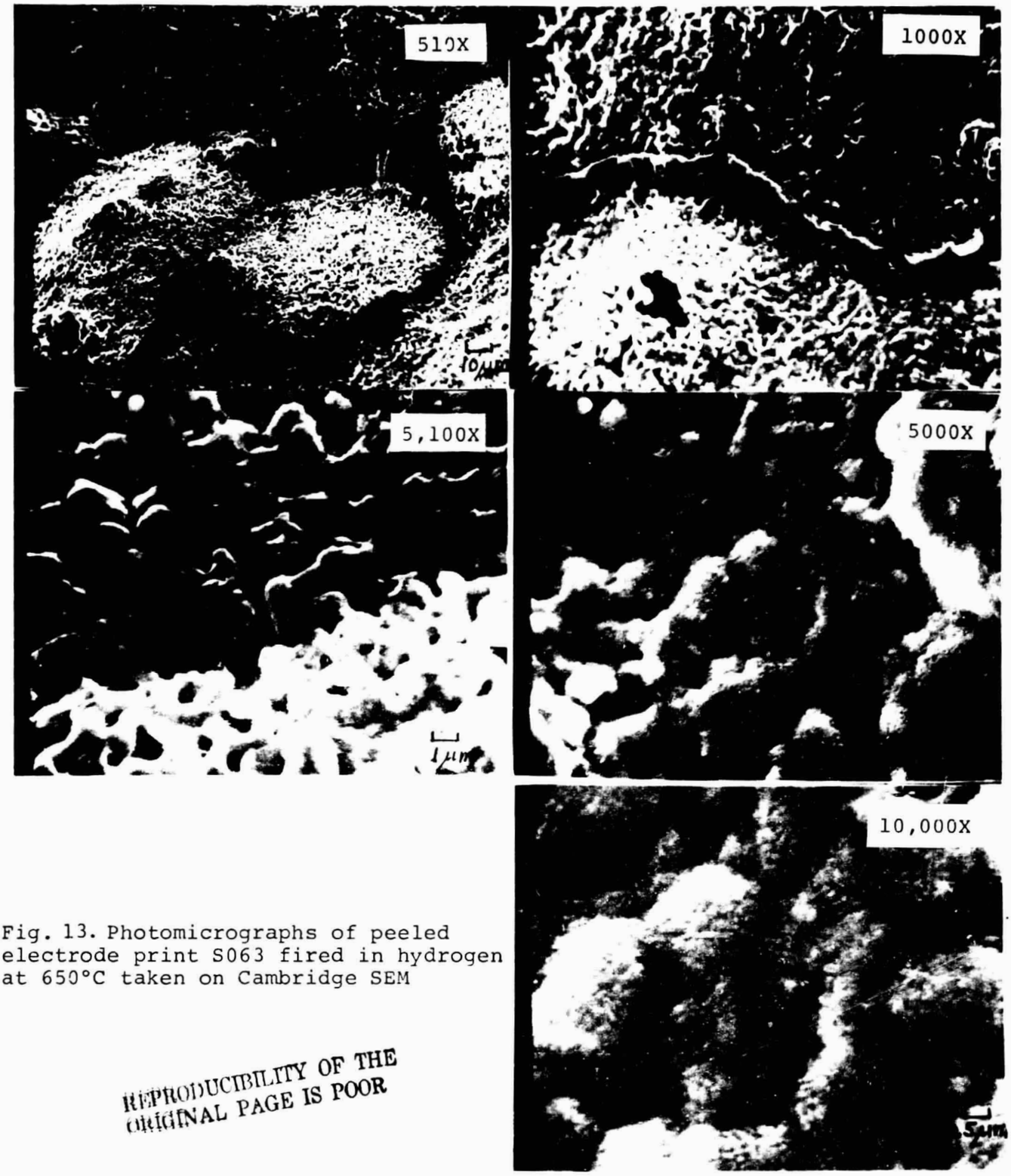

Fig. 13. Photomicrographs of peeled electrode print S063 fired in hydrogen at 650°C taken on Cambridge SEM

Fig. 14. Photomicrographs of peeled electrode of print S059 fired in hydrogen at 650°C taken on Cambridge SEM

is the same as in the case of S063, supporting the contention of oxide mixture, but the electrode appears oversintered with few voids.

Since these experiments were done, several clues made it likely that the furnace temperature is in fact higher than indicated. This was indeed the case as shown by profiling the furnace with a calibration thermocouple, which showed the center section to run almost 160°C hotter than the set point. This will be discussed in further detail in section 6.2. It is therefore likely that the inks reached a point on or near the liquidus line for the particular phase diagram.

4.3.1 Analysis of Electrical Characteristics

Cells tested consisted of four controls with titanium-palladium-silver (Ti-Pd-Ag) evaporated front and back contacts sintered at 600°C and 650°C respectively, three textured front surface cells and three cells with regular polished front surfaces. All of the surviving cells had Ti-Pd-Ag evaporated back contacts and were fired at 600°C or 650°C in hydrogen. The original curve traces are reproduced in the Appendix 2.

Of the four control cells, two showed sharp decreases in open circuit voltage, which was an even more serious problem in the experimental cells. This might be due to a junction processing problem resulting in spotty low shunt resistance. The restricted number of cells is due to a cell availability problem at the time the experiment was run.

All the experimental cells had poor open circuit voltages. The cells fired at 650°C showed open circuit voltages about half of those fired at 600°C, indicating more severe shunting at the higher temperature. Likewise, the ink containing the hydrogen-reacted Ge-Sb eutectic gave much higher open circuit voltage than the nitrogen-air reacted material (See Table 1).

Five percent of this material was combined with masterpaste S032 (93% Ag - 5% Pb and 2% AgF) to result in S064 for use on the phosphorous diffused layer. Other inks tried in this experiment were S063 (composition similar to S064 but with the eutectic alloyed in air) and S059, a p-type ink with a 5% germanium-aluminum eutectic and 1% gallium chloride. The Ge-Al eutectic is also suspect since it was reacted in a nitrogen atmosphere containing unknown amounts of room air.

Table 1. Electrical Results

PASTES	TEMPERATURES			
	600°C		650°C	
	Isc (A)	Voc (V)	Isc (A)	Voc (V)
S063	--	--	.3	.06
S064	.41	.26	.3	.13
Controls	.58	.56	.49	.52
Controls	.58	.27	.47	.12

5.0 METAL SYSTEM CONSIDERATIONS

5.1 Erratum

A letter was received from Dr. Howard Goldman of the University of Pennsylvania suggesting that the vapor pressure curve for AgF published in the first Quarterly report (Jan. 79) and the Final report (Apr. 79) was in error. The displacement between the solid and the liquid portions of the curve is unlikely for a natural phenomenon. He found an error in the cited reference and supplied a value which results in intersection of the two curve boundaries at the melting point. A representation of the curve calculated from the new values is shown in Figure 15.

Figure 15

CORRECTED*VAPOR PRESSURE OVER SILVER FLUORIDE

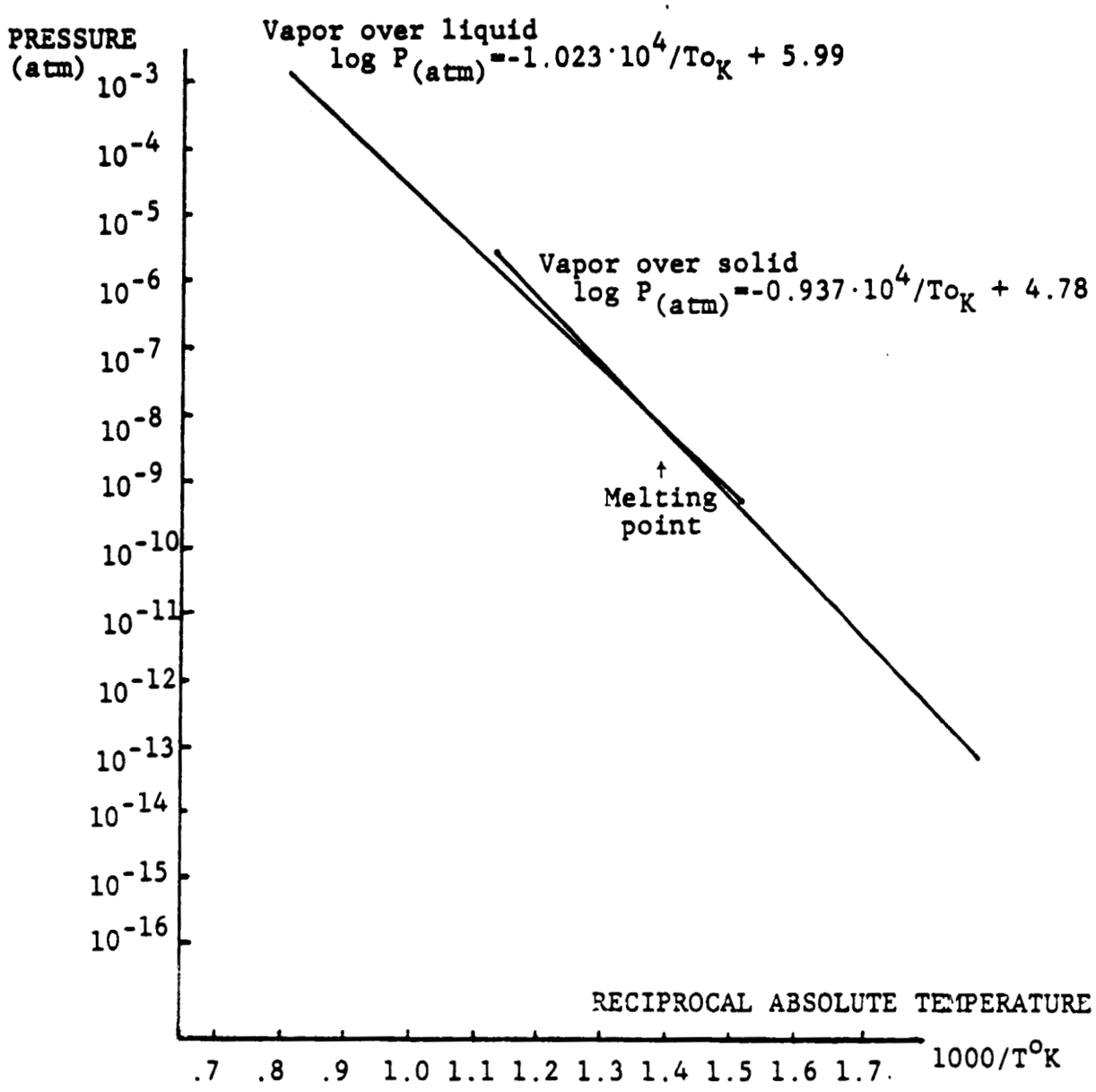

* H. Goldman, Private Comm. (Sep 1979)

5.2 Survey of Binary Alloys of Silver-Nickel and Copper

The silver-lead and silver-tin systems have been investigated previously[8] with good results in the case of silver-lead, leading to low temperature liquid phase sintering. In view of the above it is useful to review the phase diagram of this system, Fig. 16, and plot the solubility curve, Fig. 17.

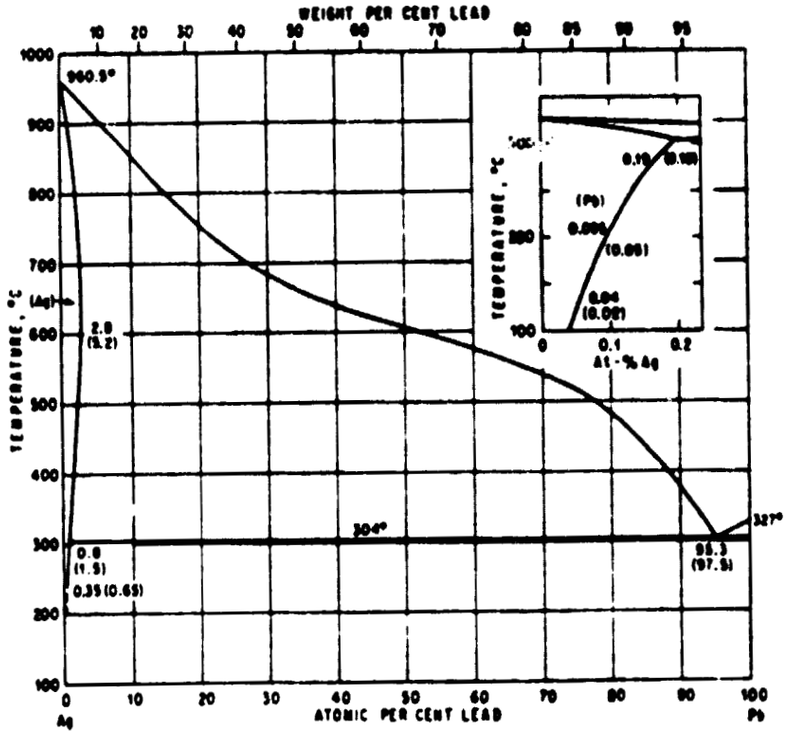

Fig. 16. Equilibrium Phase Diagram of Silver-Lead System.

The solubility of silver in the lead rich melt can be obtained from the locus of the intersections of isotherms with the liquidus curve.

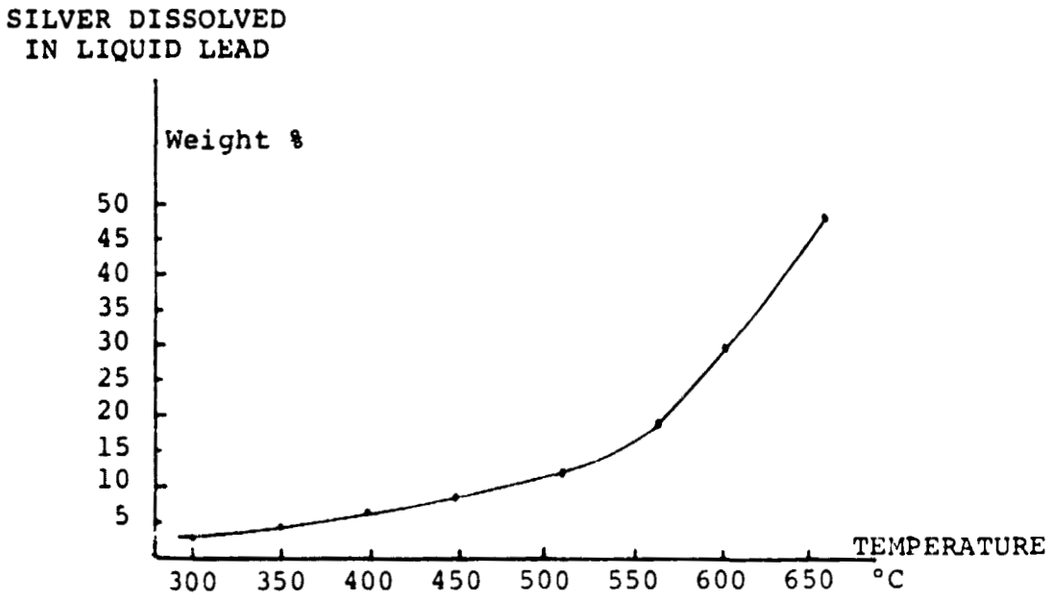

Fig. 17. Solubility Curve of Silver-Lead System.

The solubility of silver in liquid lead is quite large.

Figure 18 shows the phase diagram of the nickel tin system and Fig. 19 the corresponding solubility plot. It can be seen that the solubility of silver in lead at 400°C is almost exactly one order of magnitude higher than the nickel solubility in tin at 400°C. On the basis of solubility only, the nickel tin system does not have a high probability of success. However, it was found subsequently that solubility is not the sole parameter in getting good material transport, resulting in grain growth and a coherent continuous structure.

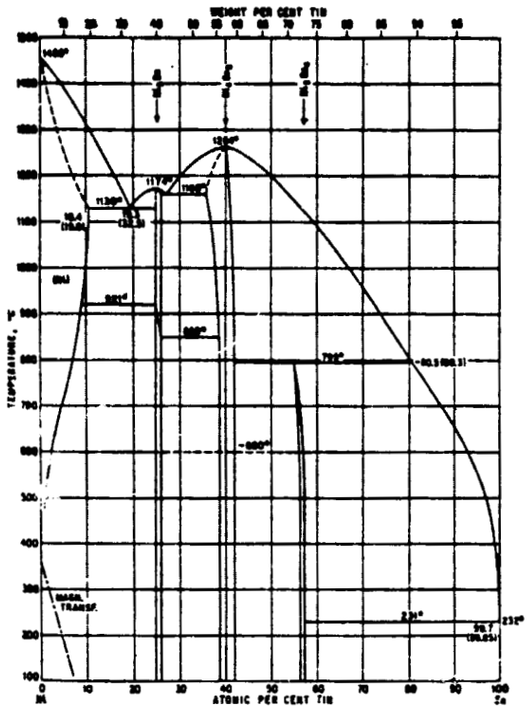

Fig. 18. Equilibrium Phase Diagram of Nickel-Tin System.

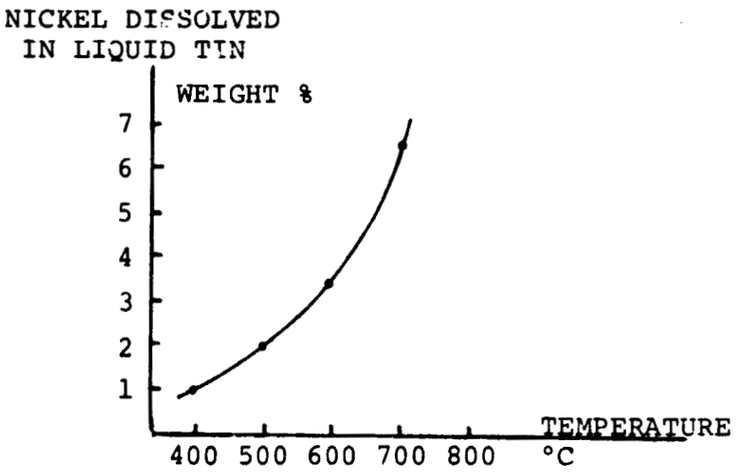

Fig. 19. Solubility Curve of Nickel-Tin System.

The phase diagram of nickel-lead is shown in Figure 20. It can be seen that a considerable miscibility gap exists. The solubility of nickel in the lead melt is given in Fig. 21 and is relatively low up to quite high temperatures.

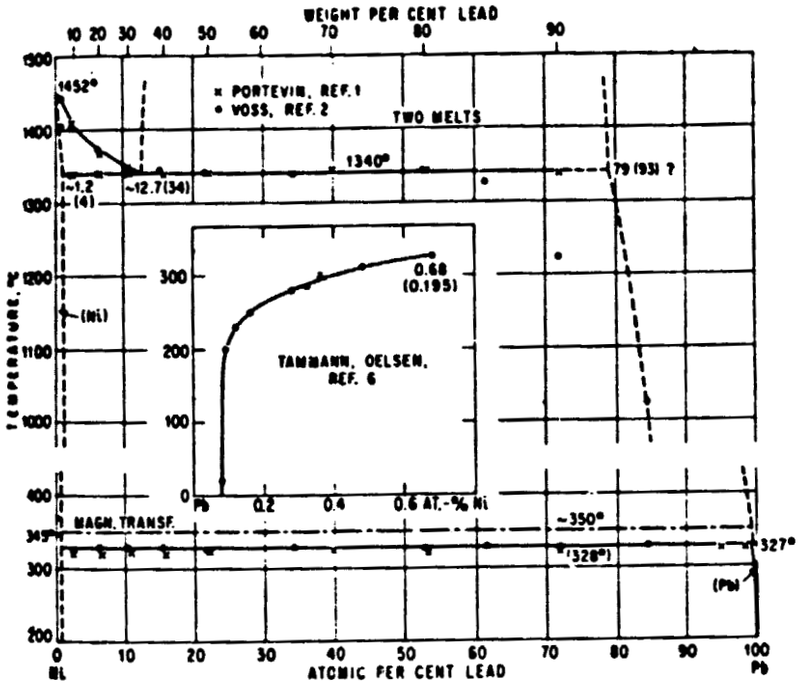

Fig. 20 Equilibrium Phase Diagram of Nickel-Lead System.

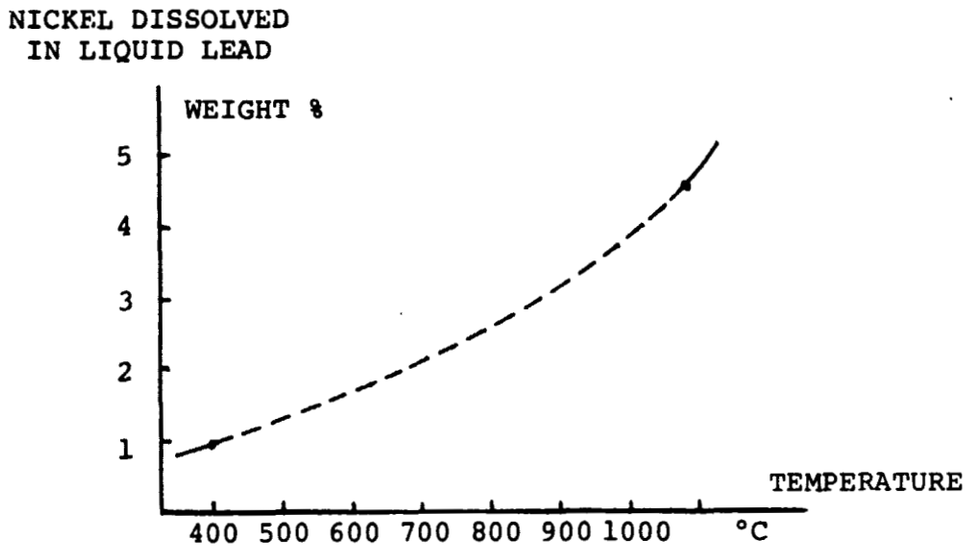

Fig. 21. Solubility Curve of Nickel-Lead System.

The dashed portion of the curve is estimated since no data was found in the literature.

A number of nickel systems have more favorable solubility factors, however they are often associated with metals having fairly high vapor pressures. Some of these are nickel-antimony, nickel-zinc and nickel bismuth. The phase diagrams of these systems are reproduced in the appendix[9].

A phase diagram of nickel-silicon is shown in Figure 22.

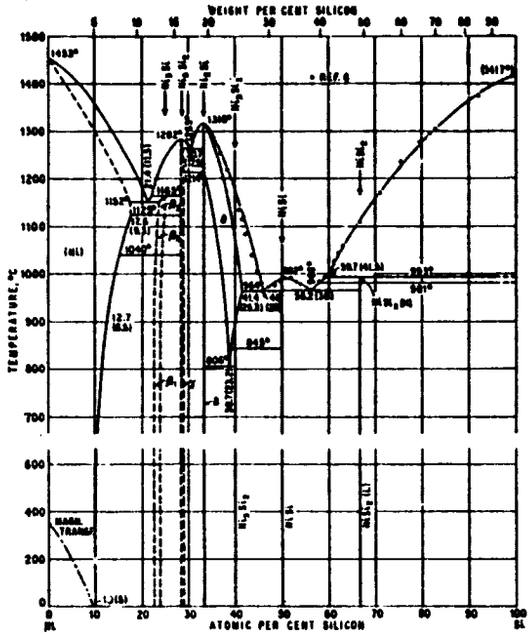

Figure 22. The nickel silicon system

Aside from its complexity, it shows the temperature of the lowest melting eutectics between silicon and nickel, which should not be approached in any firing cycles. While this is an absolute temperature limit, melting may occur at lower temperatures depending upon other additives to the paste composition such as aluminum and germanium.

The copper systems were also examined. The copper-lead phase diagram is given in Figure 23.

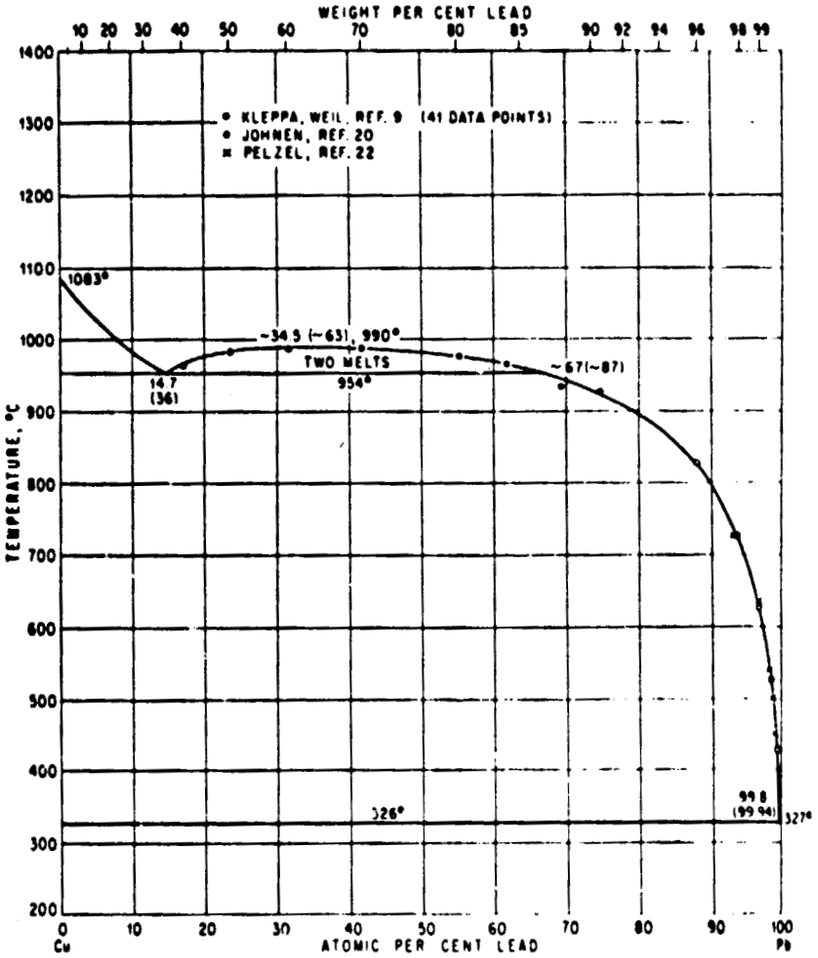

Figure 23. The equilibrium phase diagram for the copper-lead system.

The copper solubility curve in liquid lead is shown in Figure 24. Again the solubility is quite low until considerable temperatures are reached.

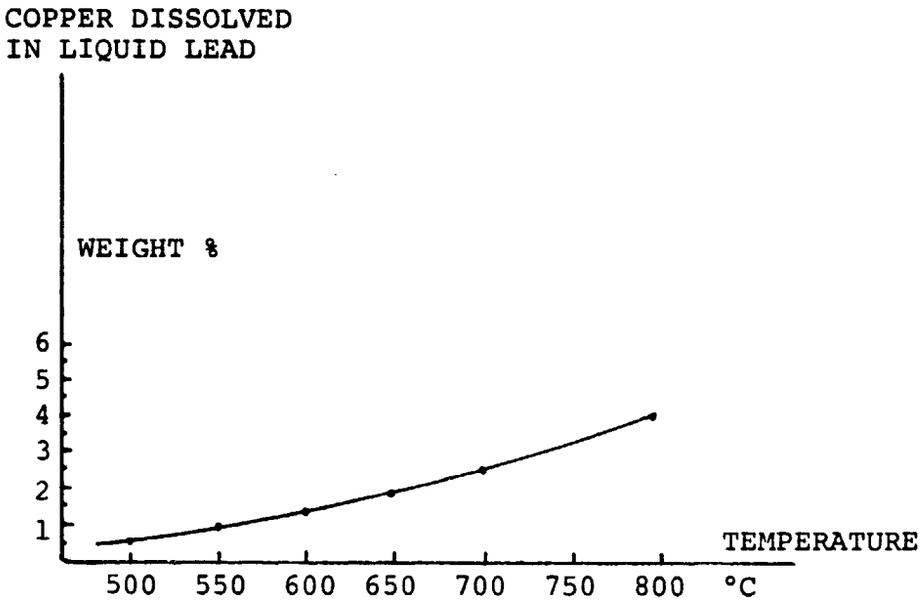

Figure 24. Copper solubility in a lead melt

Other systems again showing a higher solubility of copper can be found in the appendix. The copper aluminum system may be singled out as an interesting one, as it combines a relatively high melt solubility with a metal commonly used as doping metal in p-type silicon. However the combination of the metals tends to have severe corrosion problems in wet atmospheres.

In Figure 25 the phase diagram of silicon-copper is given to establish the upper temperature limit of thermal processes involving that system. As can be seen the absolute temperature limit of heating the copper silicon system is 802°C, however the same caveat applies as was previously mentioned with regard to potential temperature depressant additives.

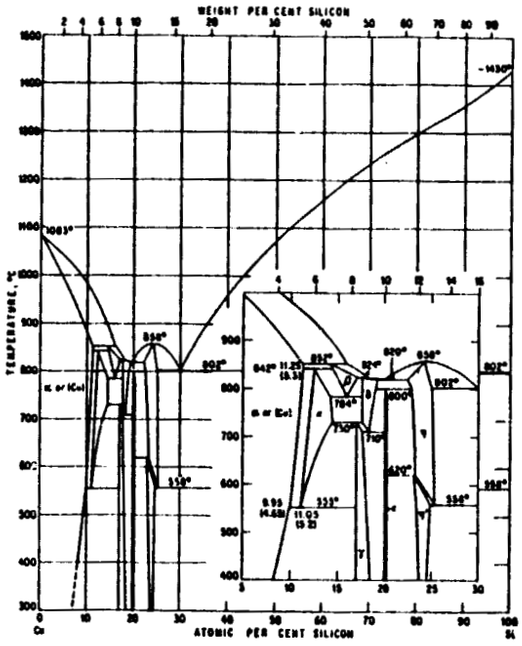

Figure 25. The Copper Silicon System

In the use of copper in contact with silicon further comments are appropriate. Copper was suspected early in semiconductor technology as the major recombination center in germanium and silicon (Collins et al[10]). Work by the present author in 1957 indicated that silicon with a high initial copper concentration introduced at high temperatures, but undergoing slow cooling suffered no minority carrier lifetime degradation[11]. Nevertheless copper in silicon devices has remained suspect for a

quarter century. A recent study of the severity of various impurities in silicon material[12] has corroborated the author's experience. Another degradation mechanism attributable to copper is its tendency to diffuse rapidly through the lattice and precipitate in clusters on defects or dislocations, leading to decoration of defects (Dash[13]). Therefore a copper spike can be driven through the space charge region of a p-n junction by allowing copper to diffuse and aggregate on an edge dislocation perpendicular to the wafer and junction. This can lead to severe junction shunting, particularly when an array of dislocations exists. Since copper is a particularly rapid diffuser, direct contact between silicon and copper should be avoided. The role of barrier metals is presently being investigated by several researchers. In any case, processing steps and structures must be carefully planned in the presence of copper metallization.

5.3 Metal Paste Preparations

Although the phase diagrams and solubility curves did not look very favorable, it was decided to do experiments with nickel-lead and nickel-tin, copper-lead and copper-tin due to the immediate availability of materials, and the benign character of lead (chemical resistance, oxidation resistance) in our experience with the lead silver system and others.

Table 2 shows the constitution of all metal inks compounded during this period.

Table 2
All Metal Pastes Fabricated
During Current Quarter

PASTE CODE	MASTER PASTE	METAL	SILVER FLUORIDE	METAL FRIT	DOPANT
S062	S032	Silver	2%	--	10% Ge-Al*, Ga
63	S032	Silver	2%	--	5% Ge-Sb*
64	S032	Silver	2%	--	5% Ge-Sb
65	"	Nickel	5%	Lead 5	0
66	"	"	"	" 10	0
67	"	"	"	" 20	0
68	"	"	"	Tin 5	0
69	"	"	"	" 10	0
70	"	"	"	" 20	0
71	"	Copper	"	Lead 5	0
72	"	"	"	" 10	0
73	"	"	"	" 20	0
74	"	"	"	Tin 5	0
75	"	"	"	" 10	0
76	"	"	"	" 20	0
77	S032	Silver	2%	Lead 5	Ti (Resinate)
78	--	Copper	2%	Lead 5	<.01%
79	S071	Copper	5%	Lead 5	4% Al-Si
80	S071	Copper	5%	Lead 5	4% Al-Ge
81	--	--	--	--	77% Al-Si
82	--	--	--	--	77% Al-Ge
83	--	Nickel	5%	--	--
84	--	"	5%	Lead 10	--

* eutectic not satisfactory

6.0 TUBE FURNACE AND GASHANDLING SYSTEM

A Heavy Duty tube furnace was acquired. The 3.7 KW furnace is designed to have a flat temperature zone of approximately 10" length with adjacent higher temperature zones compensating for end losses. The furnace is equipped with a setpoint, time-proportional controller, maintaining temperature with excursions of less than 5°C. Maximum placarded temperature is 1300°C and the unit is easily capable of reaching 1000°C (highest temperature attempted since acquisition). A quartz tube with an OD of 66mm and a length of 5 ft. (1.5m) occupies the furnace bore. Furnace and tube are pitched 3° down from the inlet end. Combustible gases can be burned off by an illuminating-gas butterfly burner furnishing a flame curtain at the open exit end of the quartz tube.

Figure 26 shows the tube furnace and gas handling system. Gases are furnished from high pressure tanks with two stage reducers and gauges. The gases are conveyed to sapphire ball flow gauges with copper tubing and through flow valves. For the nitrogen gas a ball type flow valve is used and a bellows valve is used for the hydrogen. Figure 27 shows the calibration curves for the hydrogen and nitrogen flow meters respectively. The region of instability is due to a defect in the valve at the higher flow rates. The flow meters were calibrated with the appropriate gases by allowing the gas to displace the water in inverted glass containers of known volume, partially submerged in a larger

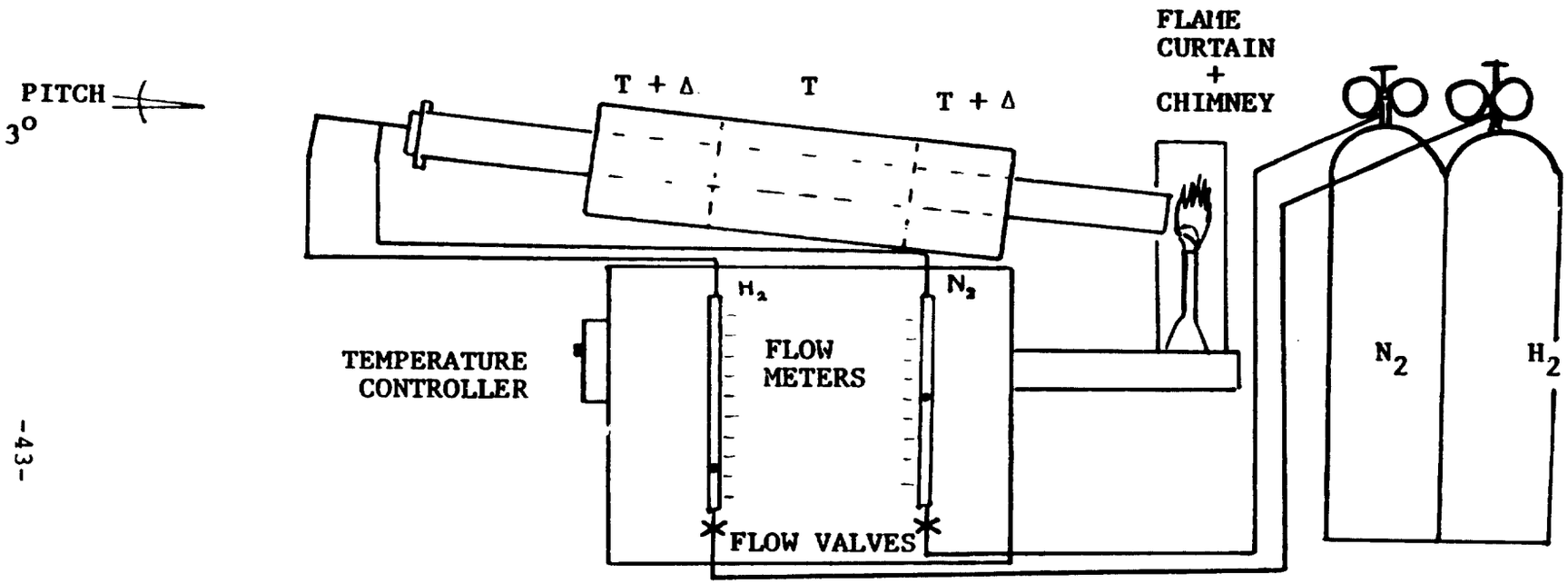

Figure 26 Tube furnace and gashandling system.

FIGURE 27

FLOW METER CALIBRATION

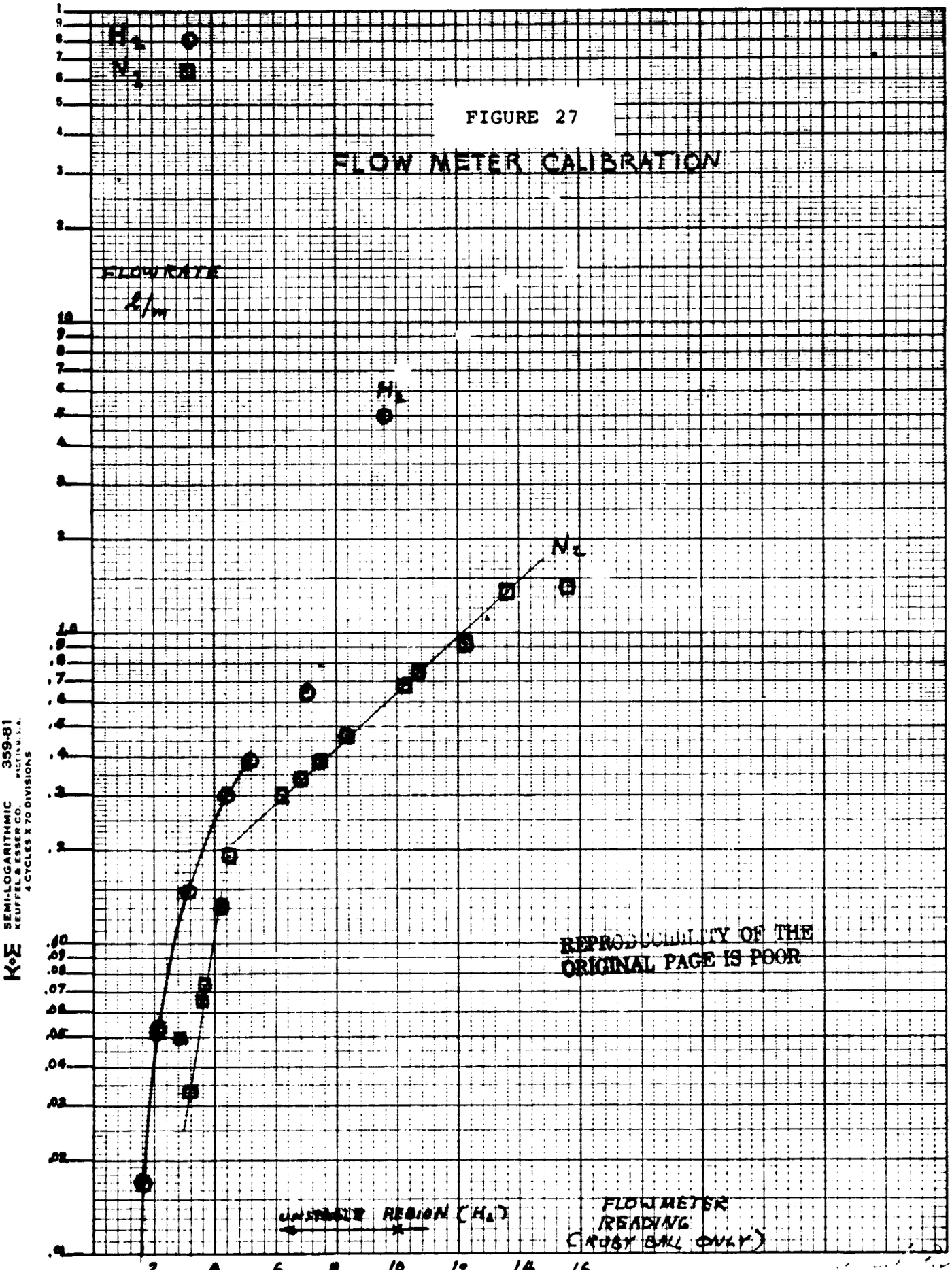

KE SEMI-LOGARITHMIC 359-81
KEUFFEL & ESSER CO. PRINTED U.S.A.
4 CYCLES X 70 DIVISIONS

container. For each flow rate the time to reach a given volume was measured on a stopwatch. While the furnace was generally adequate to the task, some problems did develop. A heating element in the inlet zone had to be rebuilt due to a short circuit to the furnace shell. A ball flow valve in the nitrogen line also had to be replaced.

6.1 Furnace Modification

During experiments with copper ink firing it was noted that copper electrodes tended to oxidize in the cooling position after being pulled from the furnace hot zone. This was due to the use of an open tube end which allowed convection to carry air as far as 6" into the quartz tube. In order to eliminate this problem 12" of 65mm quartz tubing was added to the furnace tube. The back platform with the butterfly flame curtain was extended to accommodate the new tube end position.

6.2 Furnace Temperature Profiling

In Section 4.3 it was stated that the set point temperature of the tube furnace was thought to be in error, in connection with the hydrogen firing of silver ink and their analysis. Subsequently in the firing of copper inks it again appeared that the metal layers had reached proximity of a liquid phase. The temperature profiling of the tube furnace had been scheduled earlier, but had to await availability of the equipment. Profiling was done with a calibrated chromel-alumel thermocouple of approximately 12 feet length connected to a Leeds and Northrop Speedomax slidewire potemtiometer. Temperatures were recorded on a strip chart recorder. The entire furnace was calibrated at two inch intervals, and at temperatures from 400°C to 800°C (center of furnace). An error temperature was found to range from 138°C at 400°C to 160°C above 500°C. The thermocouple was replaced as soon as a new one could be acquired. Unfortunately it is not known when the controller thermocouple failed, nor if the failure was abrupt or gradual. The fact that outer furnace control zones operated at a higher temperature (above setpoint) made the visual (color temperature) clues less effective, so that the error was not observed by the experimenter.

7.0 INITIAL EXPERIMENTS WITH NICKEL INKS

Nickel pastes S065 through S070 were screened onto undiffused N type silicon quarter wafers having a lightly etched surface. The resistivity of the material was 4.5 ohm-cm, and orientation (1,0,0). Paste compositions are reproduced from quarterly report #3 in Table 3 below:

TABLE 3

Paste #	Ni wt.%	Pb wt.%	Sn wt.%	AgF wt.%
S065	90	5	-	5
66	85	10	-	5
67	75	20	-	5
68	90	-	5	5
69	85	-	10	5
70	75	-	20	5

Each of the six inks was placed on the quartz boat, into an identifiable position. A rectangular quartz slab with longitudinal slots was used as a boat. Wafers were grouped in rows aligned vertically along the tube axis. Firing temperatures started at 500°C increasing in 50° steps to a maximum of 700°C. Nitrogen, hydrogen and forming gas (nitrogen with 10% hydrogen) were used. Gases were allowed to flow for five minutes maximum at high flow rates (about twice normal) before the boat was inserted.

Flow rates were as follows:

	N_2		H_2	
Settings	l/m	Meter Reading	l/m	Meter Reading
Nitrogen only	1.5	14	0	-
Forming Gas	1.2	13	0.15	3.2
Hydrogen only	0		0.9-5	8-10

Insertion of the boat was done in three steps. The first position was in the middle of the tube portion protruding from the furnace rear. The purpose of this step was to allow air out-gassing (2 min. 40 sec.). The second position was at the furnace exit (center of boat) for an additional 2 min. and 40 sec. This position was intended to be a prebake to eliminate the proprietary acrylic binder. The boat was then pushed to the furnace center for 8 minutes, for a total cycle time of 13 minutes and 20 seconds.

The only problem encountered in the firing was a tendency for the boat to stick to the tube at the highest temperatures. The boat could be knocked loose by sharply rapping with the hooked quartz rod used for retrieval.

7.1 Characterization of Fired Nickel Inks

The hydrogen fired inks gave the lightest gray appearance with forming gas and nitrogen yielding increasingly darker surfaces. The specimens were observed under an optical microscope (Wild-Heerbrugg) at magnifications up to 600X with and without polarized light. A discoloration was in evidence in the vicinity of the electrode boundaries. The rainbow colors made this band (seen also in the hydrogen fired specimen) attributable to transparent oxide. There was no evidence of sintering in any atmosphere or at any temperature. This was confirmed by the subsequent SEM analysis. Figure 28 shows an SEM micrograph of a green ink print. The ink is S066 containing 10 wt.% lead. Figure 29 shows ink S066 fired in hydrogen at 700°C.

In the use of the 20 wt.% tin ink S070, the fired print shows a definite decrease in average particle size. Since nickel-tin forms several intermetallic compounds, this can be used to rationalize the result.

An elemental scan was done on a S067 print fired in hydrogen at 700°C which was to have been prepared with 20 wt.% lead. No fluoresence line could be picked up for this element which should be a very efficient X-ray producer. Under the conditions of the experiment 0.15 at % Pb should have been detectable. Note Figure 30 where the lines are identified in the margins. A similar scan on S070 immediately revealed the tin line. (See Figure 31). It is intended to follow up on this problem at a later time.

Figure 28 SEM Photomicrograph of green S066 print at 900X.

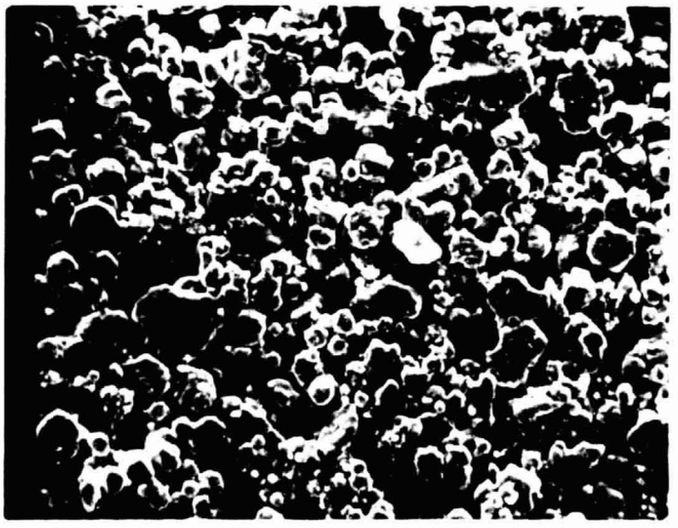

Figure 29 SEM Photomicrograph of S066 print fired in hydrogen at 700°C for 8 minutes at 950X.

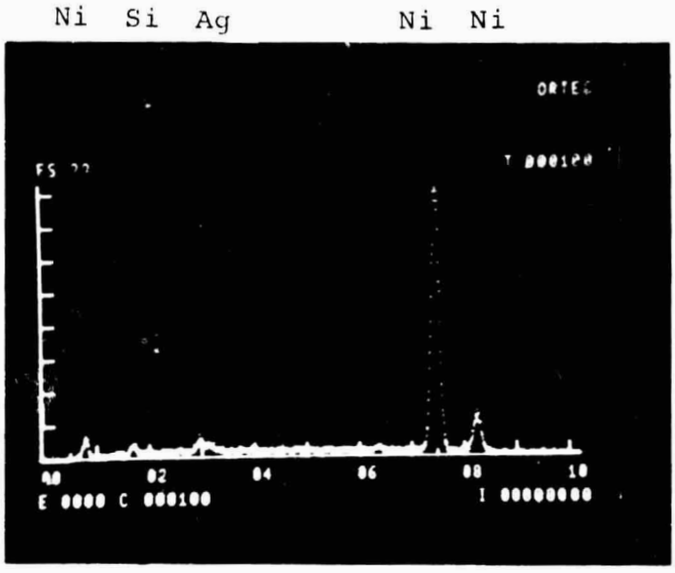

Pb?

Figure 30. Shows an X-ray fluoresence of a nickel lead (20 wt.%) ink (S067) with 100 seconds integration time.

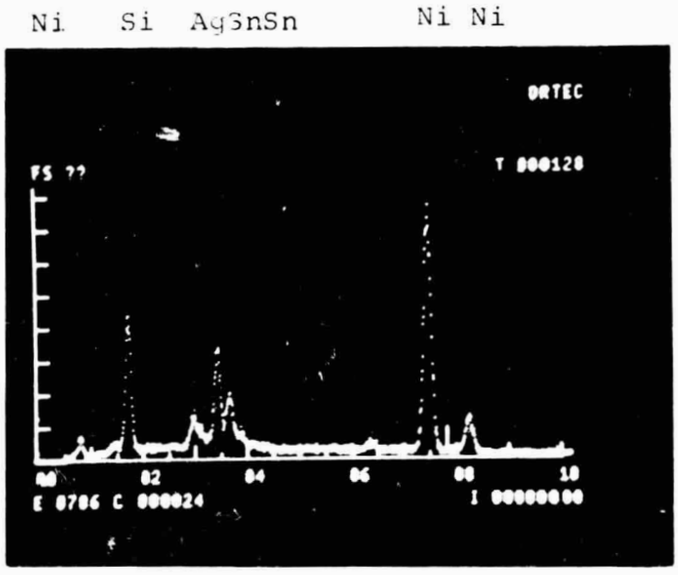

Figure 31. Similar scan of S070 containing 20% Note the prominence of the tin line.

8.0 INITIAL EXPERIMENTS WITH COPPER INKS

The following copper inks, prepared previously, were screened unto silicon wafers and fired.

TABLE 4

Ink Designation	Cu Wt.%	Pb Wt.%	Sn Wt.%	AgF Wt.%
S071	90	5	0	5
S072	85	10	0	5
S073	75	20	0	5
S074	90	0	5	5
S075	85	0	10	5
S076	75	0	20	5

During these early experiments no attempt was made to dope the materials for optimum contact to n or p type silicon, because it was desirable to observe the metallurgical properties at the fired temperatures. The temperature range of experimentation was from 550°C to 700°C in 50°C steps with the atmosphere tried previously on nickel inks (H_2, N_2+0.1H_2, N_2). The appearance of hydrogen fired materials was usually coppery-red to golden. Adhesion on all the hydrogen fired samples was very poor. The forming gas atmosphered parts were more variable in appearance, sometimes tending towards gray. Adhesion varied from questionable for the darker parts to very poor for the coppery metal deposits. The best looking electrodes were prints of S071 followed by S074 fired in hydrogen at 600°C and 700°C. However, these electrodes could be easily lifted from the silicon surface.

8.1 Characterization of Initial Copper Firing Experiment

SEM photographs of S071 and S074 fired in hydrogen at 600°C are shown in Figures 32 and 33 at two magnifications respectively. They show that both copper-lead and copper-tin materials can be sintered at relatively low temperatures. In Figure 33 bottom (S074) taken at 5600X it is shown that there is a larger spread in particle sizes (0.4μm to 4μm). However, the copper lead structure is uniform with contiguous grain boundaries, well-rounded grains indicating excellent sintering (Figures 32
It remains to determine the cause of the poor adhesion of hydrogen fired structures, which has been observed in all hydrogen fired silver inks.

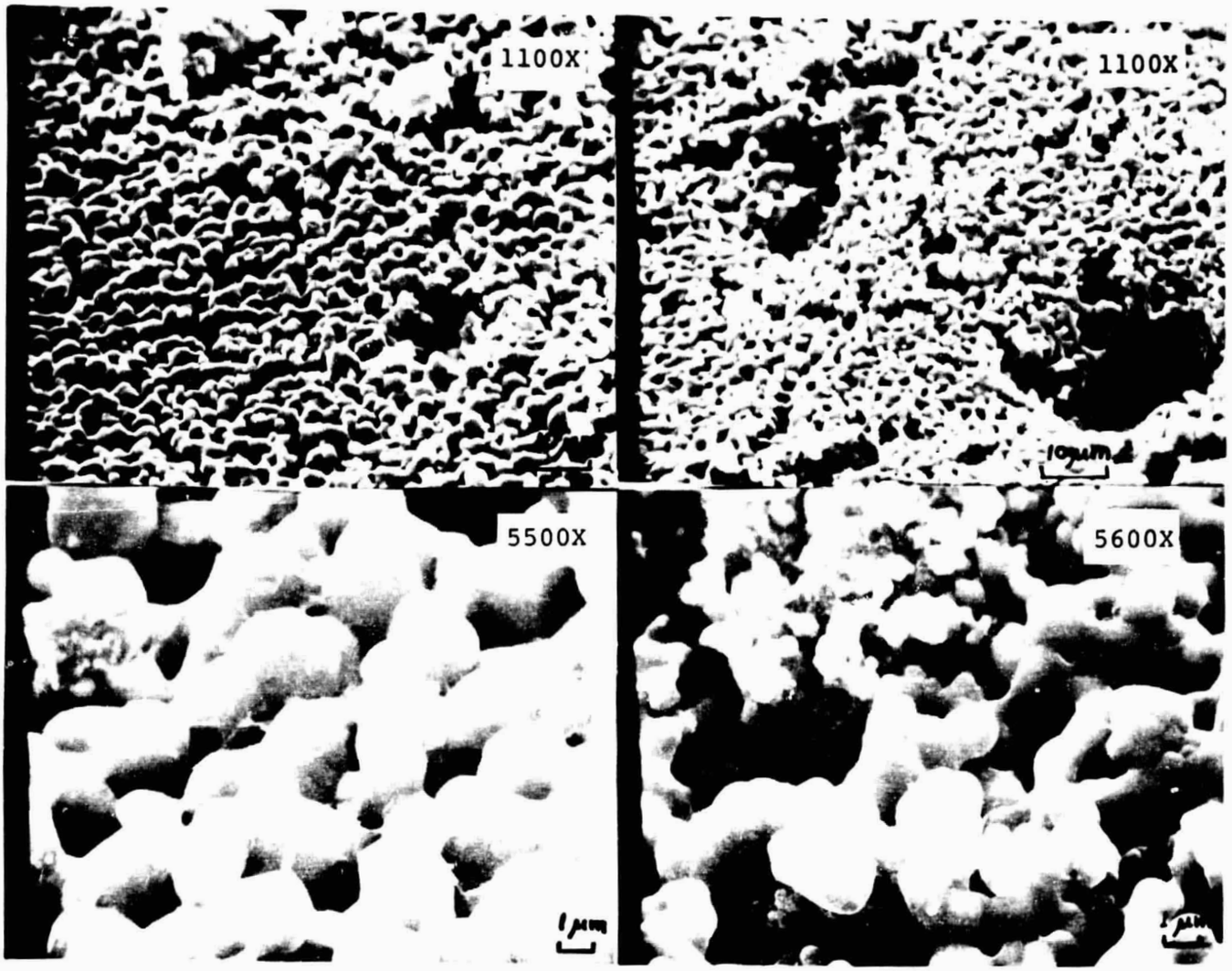

Figure 32 SEM micrograph of S071 (Cu+.05Pb) fired in hydrogen at 600°C for 8 minutes

Figure 33 SEM micrograph of S074 (Cu+.05Sn) hydrogen at 600°C for 8 minutes

9.0 SILVER-FLUORIDE-SILICON OXIDE-SILICON INTERACTION IN DIFFERENT ATMOSPHERES

Pre-oxidized polished silicon wafers with 2500Å of SiO_2 were sprinkled with silver fluoride, and subjected to a thermal cycle in different atmospheres (nitrogen, hydrogen and air). The thermal cycle consisted of pushing the specimen into the tube furnace heated to 600°C for two minutes.

A definitive result of the experiment was that the hydrogen fired silver-fluoride could not pass a scotch tape test, while the silver-fluoride residue fired in air could not be removed with an Exacto® knife. However, scanning electron micrographs did not reproduce previous conditions. Whereas previously deposits were definitely metallic (silver), residues behaved similar to insulators, showing charging effects and in some cases acting like decomposing liquids, (See Figure 34) and leaving behind a cracked surface, (See Figure 35). Intensive investigations with SEM X-ray analysis at the Automated Array Lab at Jet Propulsion Laboratory, led to the surprising result that considerable quantities of sodium (Na) are present at the surface. A subsequent wet chemical analysis showed that 12%(wt) sodium was present in the silver fluoride material as received from the manufacturer, JPL analysis showed that the ratio of fluorine to sodium was close to unity, during elemental scanning experiments. Therefore, it can be assumed that the glassy artifacts left behind on the silicon surface are sodium fluoride (melting point 993°C).

Figure 34 SEM micrograph of residue of AgF on silicon-silicon dioxide reacted at 600°C in nitrogen, at magnification 5000X.

Figure 35 Same as Figure 34 , except reacted in hydrogen, taken at magnification 900X.

10.0 REFIRING OF SILVER PASTE ELECTRODES IN HYDROGEN

A further experiment designed to investigate the lack of adhesion of hydrogen fired pastes, dealt with the sintering process in an atmosphere of hydrogen, after the fluxing action of the silver-fluoride decomposition. For this purpose a previously sintered silver electrode S026 was subjected to a heat-treatment in a hydrogen atmosphere (600°C for 10 min.).

Figure 36 shows the print after the hydrogen treatment and Figure 37 shows the untreated controls. Both the treated speciment and the controls passed a scotch tape test and a scratch resistance test.

The above experiments suggested that a two-step firing process utilizing an inert atmosphere for AgF decomposition and hydrogen for the sintering step might produce the desired combination of good adhesion and cohesion.

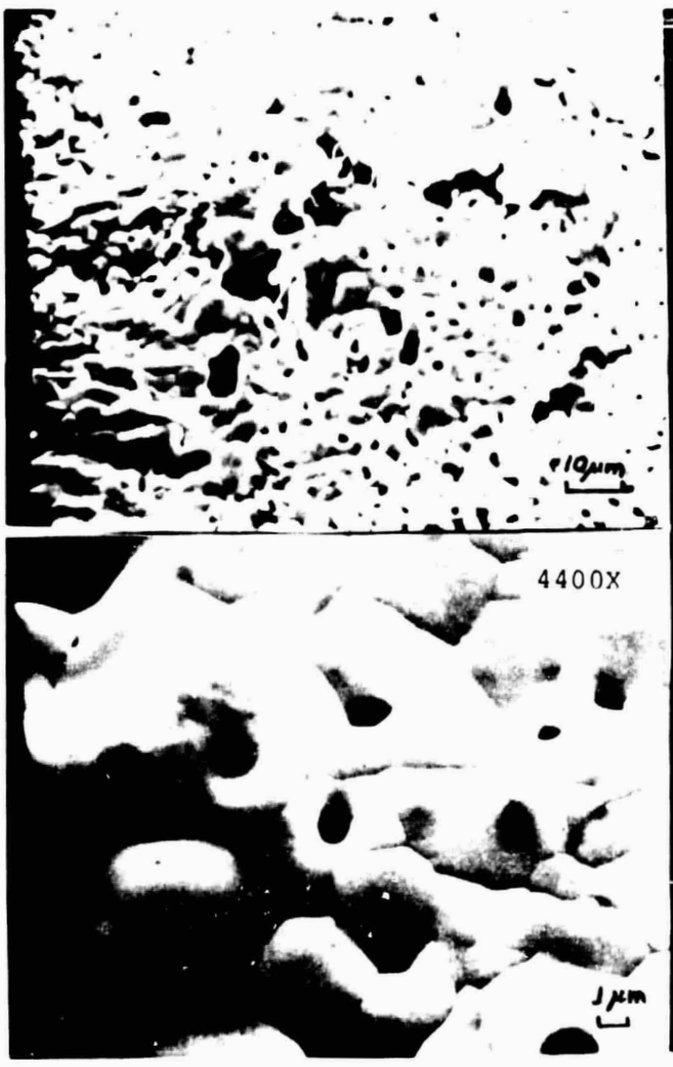

Figure 36 SEM micrograph of S026 (Ag+.05 Pb) refired in hydrogen for 10 minutes

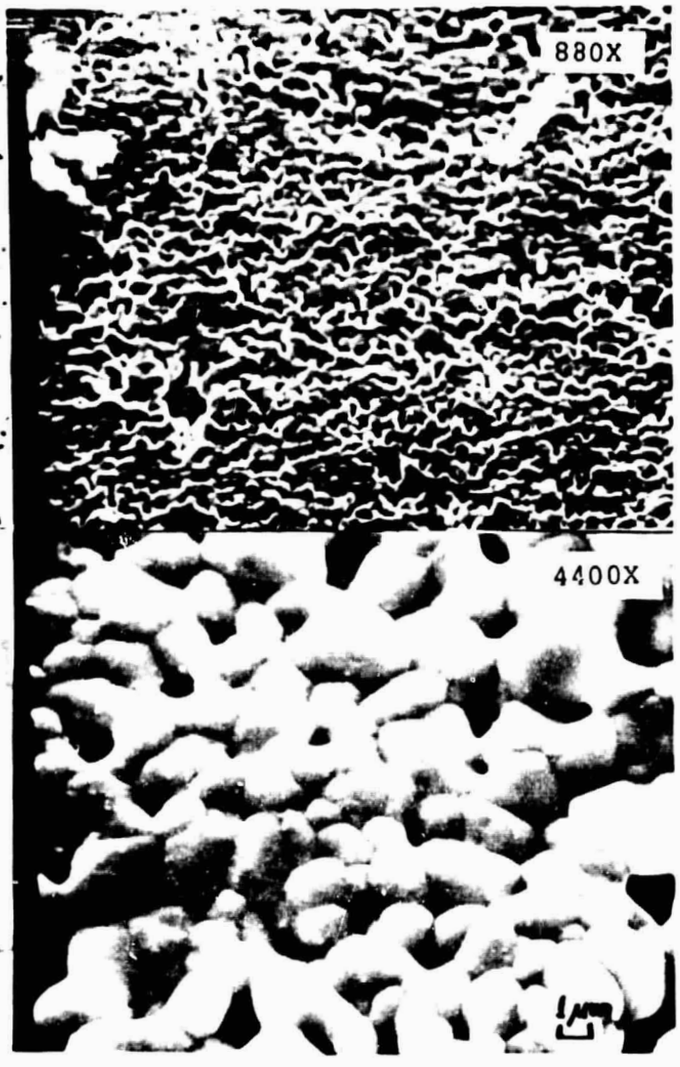

Figure 37 SEM micrograph of original S026 paint used as control for Figure 36

11.0 TWO STEP FIRING PROCESS

11.1 Two Step Firing Experiment of a Silver Ink

Silicon wafers screened with S071 (Cu + 5 wt.% Pb) were subjected to 10 min. heating at 710°C followed by 4 minutes in hydrogen. During the change of gases the boat was pulled to the furnace exit in order to prevent an excessive thermal dwell in nitrogen. The nearly black electrodes could be observed through the quartz tube. Shortly after hydrogen flow commenced they returned to a bright coppery color (estimated temperature of wafer ∿300-400°C). The electrodes were extremely adherent and cosmetically attractive.

12.0 FURTHER COPPER PASTE EXPERIMENTS

A second set of experiments was done with the following inks:

TABLE 5
Additional Copper Pastes

Product Code	Copper wt%	Silver Fluoride wt%	Lead wt%	Dopant wt%
S071	90	(Hudson) 5	5	------
S077	99.94 S032	(Silver Master Paste)		.06 Ti Resinate
S078	93	(Hudson) 2	5	------
S079	96 S071	---	--	4 Eutectic Al-Si
S080	96 S071	---	--	4 Eutectic Al-Ge

All the above with the exception of S077 were screened as linear test patterns on nominally 2 cm p-type silicon wafers (solar cell material). Wafers were then fired in the two step firing process reported in the last section. The flat quartz boat with wafers held loosely in grooves, was first positioned close to the furnace exit to remove the paste vehicle (drying) in nitrogen. Then the boat was positioned in the center of the furnace set at 500°C with a nitrogen flow of 1.5 liters/min. for 5 minutes, in order to activate the silver fluoride. Subsequent sintering took place in flowing hydrogen at 50°C intervals (500°C to 700°C) for 8 minutes.

Figure 38 shows a sequence of SEM photomicrographs of copper ink S071 fired in the two step process as a function of temperature at two magnifications. It can be seen that at the lowest tempera-

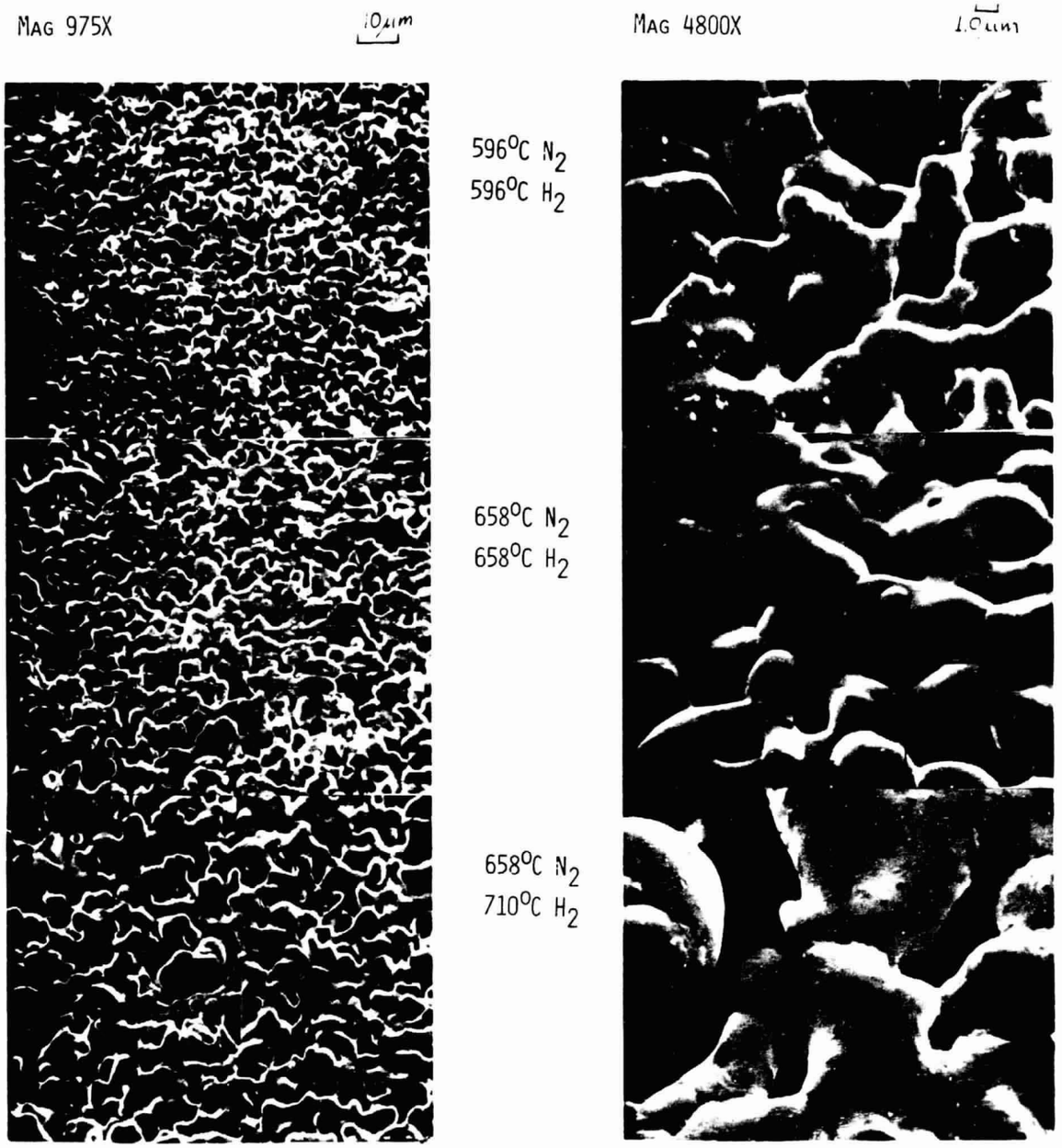

FIGURE 38 SEM PHOTOMICROGRAPHS OF S071 COPPER INK CONTAINING 5% AgF AND 5% Pb, AS A FUNCTION OF TEMPERATURE.

ture (596°C corrected) the grain size is considerable indicating a lower firing temperature to be more optimum.

Figure 39 shows micrographs of paste S079 and S080. These are similar to S071 except for the 5% additions of eutectics aluminum-silicon and aluminum-germanium respectively. On the left hand side of Figure 39 is a temperature sequence up to 860°C. The highest temperature shows incipient melting which is to be expected as the copper-silicon eutectic temperature is 802°C. The temperature labels on these figures are corrected, based upon the temperature profiling (Section 6.2). The target temperatures were 500°C, 600°C and 700°C.

The right column in Figure 39 shows the upper row portion at a higher magnification (4800X). The electrode is actually over-sintered, approaching the appearance of a solid sheet. The lower photograph in this column shows a fired print of S080. This print experienced firing conditions similar to the one pictured in the top left hand column, but shows even more advanced sintering. This suggests that the germanium eutectic addition lowers the overall melting point of the paste.

S078 employing 2% AgF as scavenger (similar to the silver pastes) had poor adhesion. This is in contrast to the silver inks in which 2% AgF proved quite adequate for good mechanical bonding. Therefore copper paste formulations prepared subsequently always employed 5% AgF.

MAG 975X

N760°C
H658°C

MAG 4800X

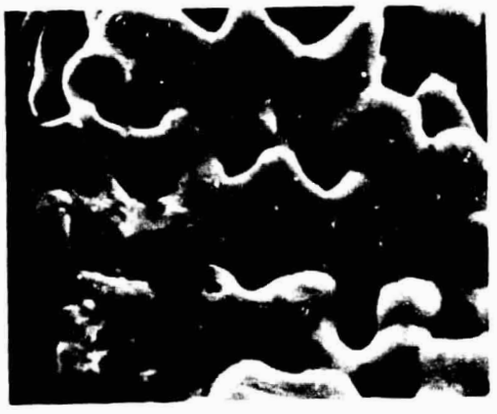

N760°C
H760°C

MAG 975X

N760°C
H860°C

N760°C
H658°C

FIGURE 39 SEM PHOTOMICROGRAPHS OF COPPER INKS S079 CONTAINING 5% AgF, 5% Al-Si EUTECTIC AND 5% Pb AS A FUNCTION OF TEMPERATURE. THE SECOND PHOTO IN THE RIGHT COLUMN SHOWS SIMILAR INK S080 WITH 5% Al-Ge EUTECTIC INSTEAD OF SILICON (COMPARES TO UPPER LEFT PHOTO).

12.1 Characterization

Measurements of contact resistance were done by the Shockley method. The lowest contact resistance determined in this was $1 \cdot 10^{-3} \Omega cm^2$ at a firing temperature of 600°C. Series resistance measurements were obtained from the voltage drops of the current bearing electrodes. Lowest series resistances were on the order of 6Ω at a firing temperature at 600°C.

Solderability experiments were performed with a soldering iron and rosin core 63-37 tin-lead solder. The electrodes soldered easily and there was no tendency to lift the copper layer. A current electrode on the linear array was solder coated to a thickness of 0.71mm and was then pried off with an Exacto knife. Approximately 20% of the electrode area pulled silicon out of the wafer substrate.

Optical microscope examination of specimens of S071, S079 and S080 fired at the highest temperatures (700°C) appeared to indicate incipient melting as shown by discoloration and the existence of small shiny spheres. Since the binary eutectics expected with these inks occur at higher temperatures (802°C for copper-silicon) it was felt that furnace temperatures may be incorrect in the direction of higher temperature.

13.0 FURTHER NICKEL INK EXPERIMENTS

The initial nickel paste experiments described in section 7 did not show any sintering action. The nickel-tin system in our experimentation showed a particle size decrease as a function of temperature which was attributed to the possible formation of nickel-tin intermetallics. While this is definitive negative information, ruling out the use of the nickel-tin system for application to base metal pastes, the same point could not be made for the nickel-lead system. In that case no sintering was observed, nor could the lead component (20 wt%) be detected in an X-ray fluorescence elemental scan. Since the detectability limit for lead with this instrumentation is 0.15 wt%, it was suspected that the lead component was inadvertently left out of the paste mix. It was therefore decided to rerun the experiment and to fabricate pastes S083, and S084 again, containing 5 wt% and 10 wt% lead respectively. No attempt was made to dope these inks as these were to be metallurgical tests only. The pastes were screened unto silicon wafers and fired by the two step process described in a previous section. The top row in Figure 40 shows the SEM appearance of the prints after the nitrogen portion of the process, done at 658°C for 5 minutes. (The temperature given has been corrected for the thermocouple error reported in section 6.2.) The particle size averages about 0.3μm and there is no evidence of sintering, in that there is no coalescence of grains. The bottom row shows the SEM micrographs after

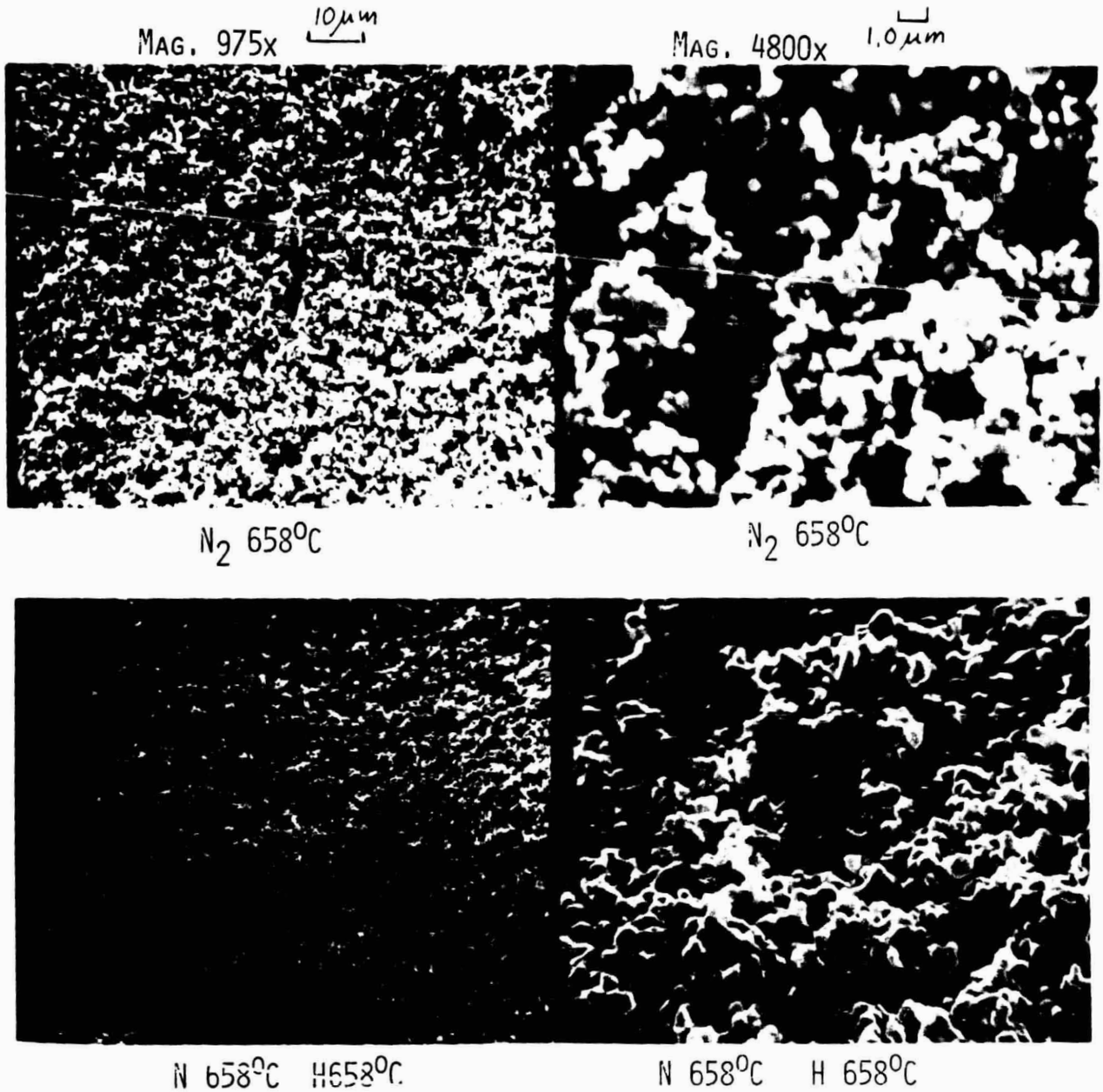

Figure 40 SEM Photomicrographs of S084 nickel ink containing 5% AgF and 10% Pb upper row fired in nitrogen only 5 minutes, lower row in nitrogen 5 minutes, hydrogen 10 minutes.

the additional hydrogen firing step (10 minutes). In this case definitive sintering can be observed. Figure 41 shows SEM micrographs of the same paste S084 fired in the two step process at higher temperature. Sintering in the case of the 760°C temperature is quite adequate with a particle size of $\sim 2\mu m$. The middle row shows signs of being oversintered.

At lower magnification (middle, left micrograph) cracks can be seen. This can be attributed to a strong bond at the silicon-nickel interface, and low tolerance to deformation of the sintered nickel sheet due to the oversintered, solid sheet nature of the electrode.

The lowest row of photographs shows a portion of a print of S084 with 5 wt% Pb on the right side. The line spectrum is shown on the left hand side, bottom row. In this case the lead Pb_M line at 2.35 KeV can be seen under the solid cursor line. This serves as additional evidence that the previous nickel paste experiment was defective in that the frit metal lead had been omitted.

Figure 42 shows views of S083 and S084 fired at the same temperature. The lower micrograph shows a larger grain size, corresponding to the larger lead addition (10% as compared to 5%). The grain growth appears to scale with the amount of frit metal (2x).

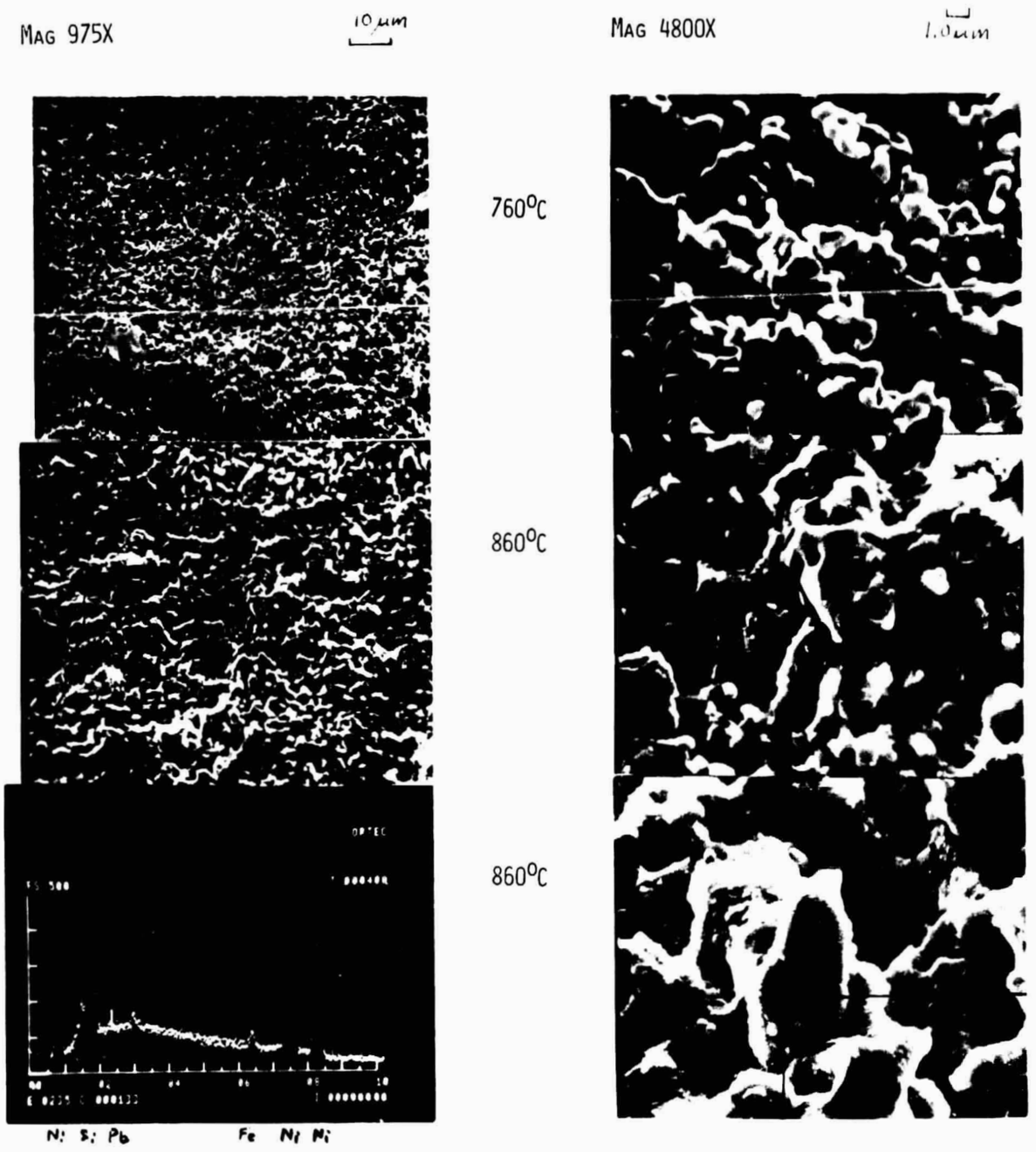

FIGURE 41 SEM PHOTOMICROGRAPH OF S084 NICKEL INK WITH 10 WT% LEAD, TOP AND MIDDLE ROW, AND S083 NICKEL, 5 WT% LEAD BOTTOM ROW, NOTE Pb_M LINE AT 2.35 KeV.

MAG 975 10μm

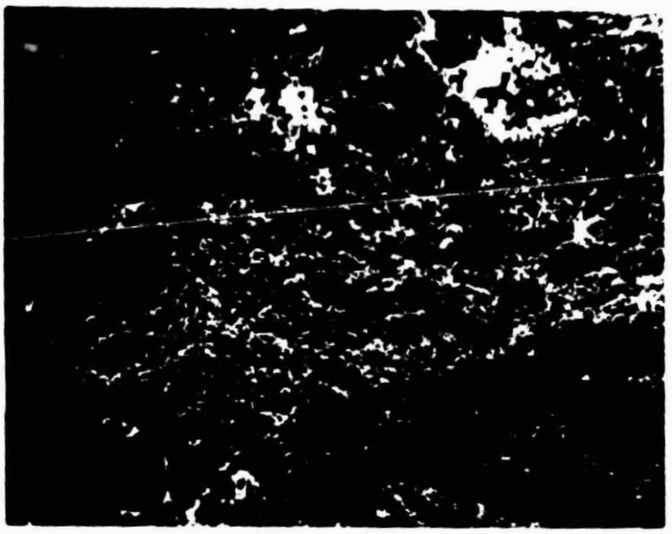

S083

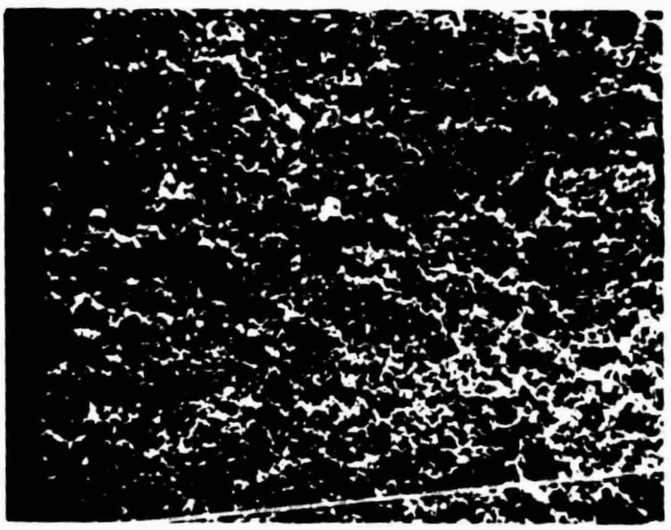

S084

Figure 42 Comparison between the SEM micrographs of nickel inks S083 5% Pb and S084 10% at same temperature and magnification (760°C, 975x). The lower photo with the larger lead addition appears to show more grain growth and coherence.

14.0 SOLAR CELL EXPERIMENT WITH COPPER INKS

Only a single solar cell experiment could be run with the base metal inks in the contract time remaining. Pastes S079 and S080 containing copper, 5 wt% Pb, 5 wt% AgF, 5 wt% Al-Si eutectic and 5 wt% Al-Ge eutectic respectively were screened onto the backsurfaces of nominally 2Ωcm p type solar cell wafers of 2 1/4" diameter. The phosphorus diffused cells with a nominal junction depth of 0.3μm had no back surface field and a wafer thickness of 300μm. The first group tried, had a front contact of Ti-Pd-Ag. It was then determined from the control cells that the Ti-Pd-Ag front contact was responsible for junction shunting, even at the lowest firing temperatures used (550°C). Therefore the next group of cells was screened and fired prior to the front contact placement.

Cells were screened and fired in a tube furnace at the facility of Applied Solar Energy Corporation (ASEC). They were activated in nitrogen for 5 minutes and then sintered in hydrogen for 8 minutes. Additional groups were fired for equivalent times at 650°C and 750°C. Cells were placed on flat quartz boats with about 20% of the wafer area overhanging the boat edges. After withdrawal from the tube the overhanding segments of the copper electrodes showed signs of oxidation. This was attributed to a rather short quartz tube being in use at ASEC. The oxidation at 550°C was not sufficiently severe to be detectible (except

possibly by comparison to a nonoxidized copper screened wafer).

Cells were then placed in an AM1 light tower and curve traced. The results are shown in Figures 43,44(raw data). Three of the IV traces are practically congruent, yielding about 9.4% AM1 efficiency without AR coating (28°C).

The maximum IV curve (9.4%) includes electrodes made from both S079 (Al-Si eutectic) and S080 (Al-Ge eutectic) showing that cell characteristics are not limited by either contact. Figure 43 gives the test results of cells in which the front contact was applied after firing the back contact. The cell fired at 650°C (S080) indicates a severe loss in both open circuit voltage and short circuit current at that temperature. Surprisingly the fillfactor is still reasonably good, 0.69, compared to 0.745 for the cells fired at 550°C, S080 paste fired at 750°C shows a catastrophic decrease in open circuit voltage from 0.585 V to 0.270 V. The optimum firing temperature for these inks remains to be determined.

Figure 44 gives the characteristics of cells in which the front contact experiences the same heat treatment as the back contact. Note that the control cell has the lowest maximum power point voltage and open circuit voltage. This is somewhat fortuitous as the other cells had a similar front contact and identical heat treatment. Additional curves may be found in the Appendix A.5.

FIGURE 43

11/29/76

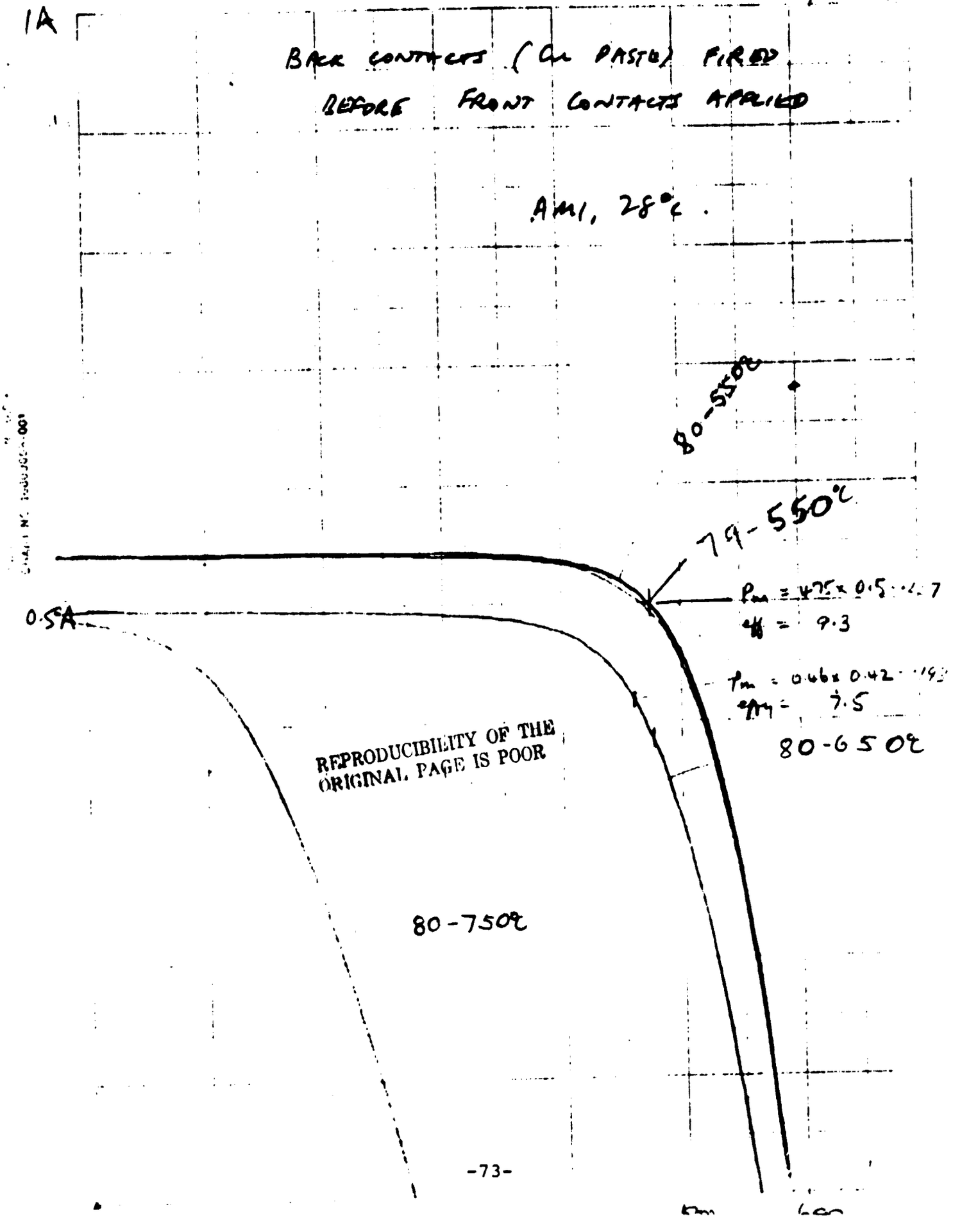

FIGURE 44

11/29/79

550°C HT

AM1, 28°C

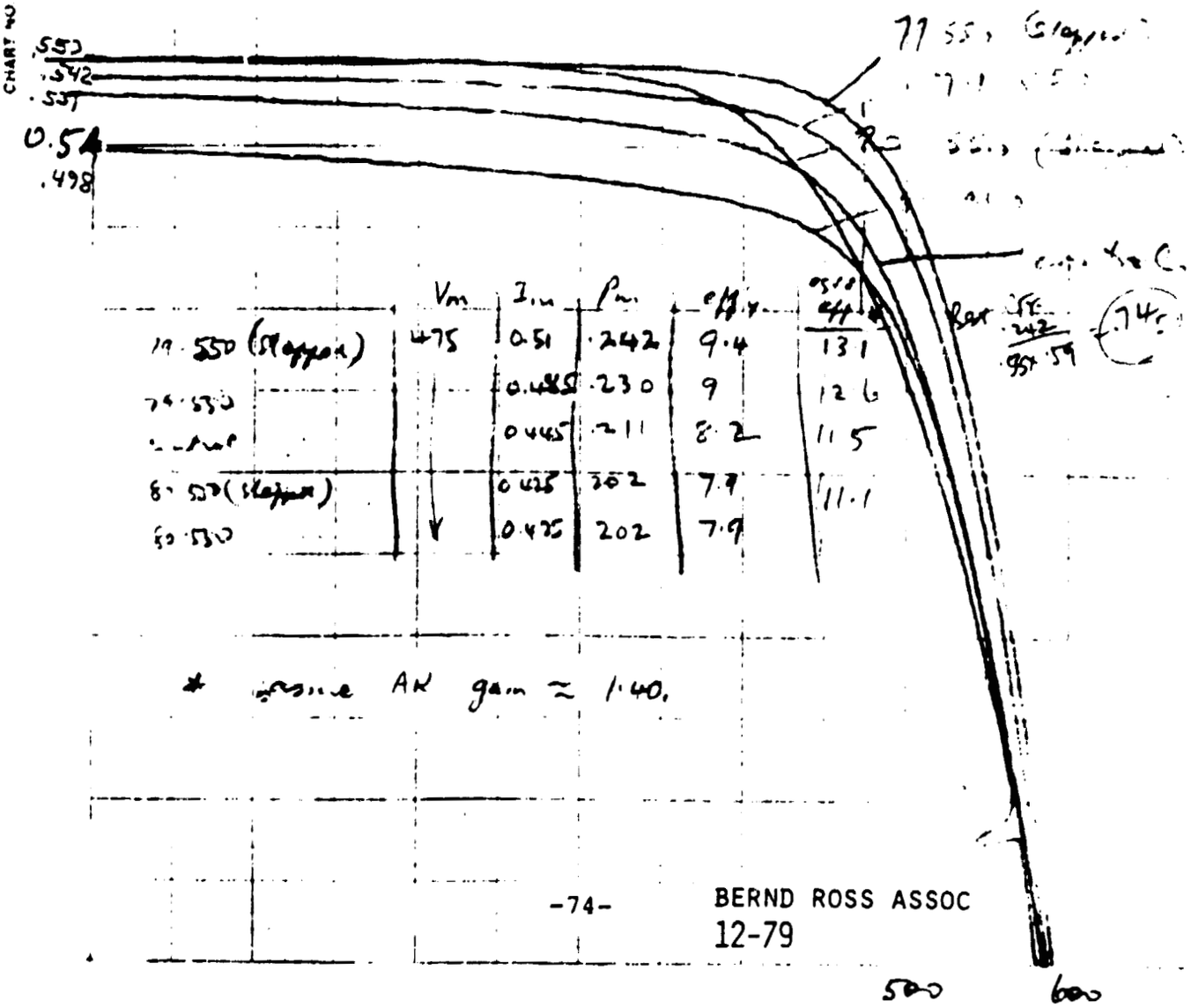

	V_m	I_m	P_m	eff.	95% eff.
19 · 550 (slippage)	.475	0.51	.242	9.4	13.1
79 · 550		0.485	.230	9	12.6
[illegible]		0.465	.211	8.2	11.5
8 · 537 (slippage)		0.425	.202	7.9	11.1
60 · 550	↓	0.425	.202	7.9	

* [illegible] AM gain ≈ 1.40.

Time did not permit experimentation with front contacts. It is recommended to try these pastes on front contacts in the normal fashion as well as in solar cells with SiO_2 and other AR coatings. Since the efficacy of the oxide scavenger for removal of SiO_2 is a matter of record it is believed that additional process economics can be achieved by applying the front contact last.

15.0 CONCLUSIONS AND PROBLEMS

A base metal contact for solar cells has been demonstrated which appears to meet the technical and cost objectives of this effort. Environmental qualities and life expectancy of the copper contact remain to be determined. Further economies are feasible due to a good probability of allowing the front contact to be applied after the AR coating.

Metallurgically it has been shown that the nickel lead system is a good candidate for a base metal contact.

I was shown that, in the case of copper, the eutectic additions, allow good ohmic contact properties for low temperature processed screened contacts. A two step process of atmosphere firing has given good results in the case of copper and nickel. Silver contacts fired in the two step process to maintain the metallic state for titanium and antimony, were non-adherent.

A method for specific contact resistance measurement for screened contacts was developed, but sufficient experience was not gained to allow rating its credibility and accuracy. This was due to continued malfunction of the associated digital voltmeter. A new instrument has since been acquired.

A major calibration problem with the furnace control thermocouple made some previous experiments ambiguous in the temperature para-

meter. A platinum-platinum + rhodium calibration thermocouple along with electronic instrumentation has been purchased to eliminate recurrence of this problem.

16.0 RECOMMENDATIONS

Further work should be done with front contact aspects of the copper contact as well as optimization of firing temperature, required amounts of eutectic additions, and required amounts of silver fluoride addition.

The nickel-lead system still appears to be a good candidate for solar cell contacts and should be further investigated.

While the economic aspects of silver make it considerably less attractive at this time, and even less so in the future, it is of at least academic interest to make its electrical properties as an all metal ink more adaptable to solar cells.

A central problem remains the possible interaction of the copper contact with the silicon lattice, the existence of a potential diffusion barrier and the life expectancy of the contact.

17.0 NEW TECHNOLOGY

New Technology reports were filed as follows:

1) Four oxide scavenger materials that can be incorporated in the metal paste, remove silicon oxide during the firing step and leave no harmful residues.

2) Use of frit metal coated powders on the all metal, screenable electrode systems, such as lead plated copper powder or lead plated nickel.

3) Use of eutectic alloy powders of semiconductors and doping metals in screenable, all metal electrode systems.

4) A two step firing system employing the successive use of different furnace ambient atmospheres, to provide optimum conditions for (1) oxide scavenger material activation and (2) major constituent powder grain sintering.

18.0 PROGRESS ON PROGRAM PLAN

PROGRAM ACTIVITY		MONTHS AFTER EXTENSION							
PHASE I 1.0		J	J	A	S	O	N	D	
PHASE II 2.0		1	2	3	4	5	6	7	8
1.1	Ohmic Contact Optimization	▽			△				
2.1		▽							△
1.2	Contact Conductance		▽	△					
2.2			▽	△					
1.3	Pull Test			▽	△				
2.3					▽	△			
1.4	Temperature Humidity Cycle			▽		△			
2.4						▽	△		
1.5	Solder Leach Resistance					▽	△		
2.5							▽	△	△
1.6	Firing Temperature-Time Optimization		▽	△					
2.6	Firing Temperature-Time-Atmosphere Optimization					▽	△		
1.7	Vehicle Percent Solids Optimization		▽	△					
2.7						▽	△		
1.8	Monthly Reports	⊙		⊙	⊙	⊙			
1.9	Quarterly Reports		⊙				•		
1.10	Review Meetings			×	×		×	×	
				PIM				PIM	

19.0 APPENDIX

APPENDIX A.1a

Figure 45

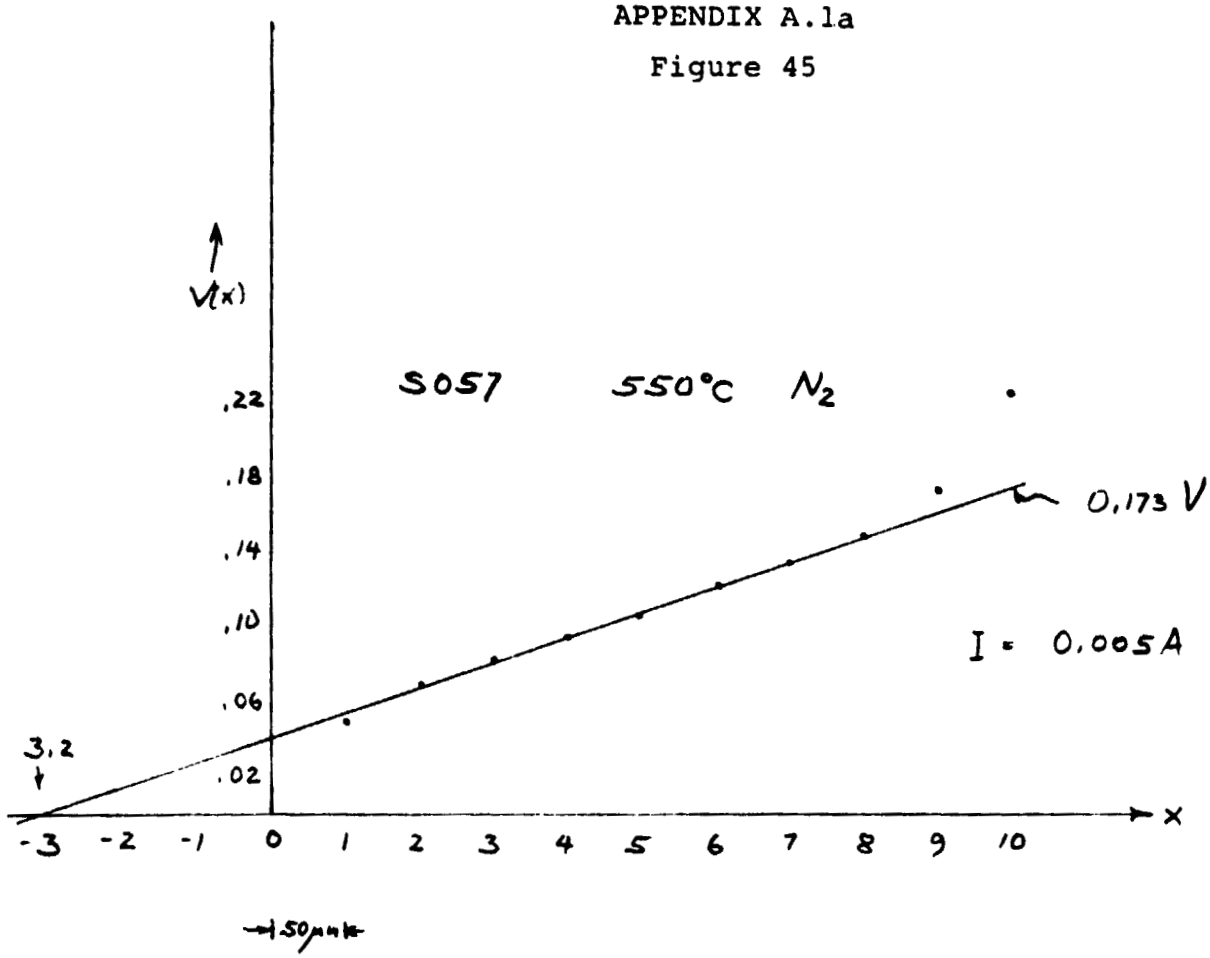

$$R_\square = \frac{0,172\,V}{0,005} \cdot 0,10 = 3,46\,\Omega/\square \quad (\text{Eqn. (1) p. 10})$$

$$R_c = L_T^2 R_\square = (3,2 \cdot 50 \cdot 10^{-4}\,cm)^2 \cdot 3,46\,\Omega/\square$$

$$= 8,86 \cdot 10^{-3}\,\Omega\,cm^2$$

SAMPLE PLOT + CONTACT RESISTANCE CALCULATION

A.1b

Figure 46

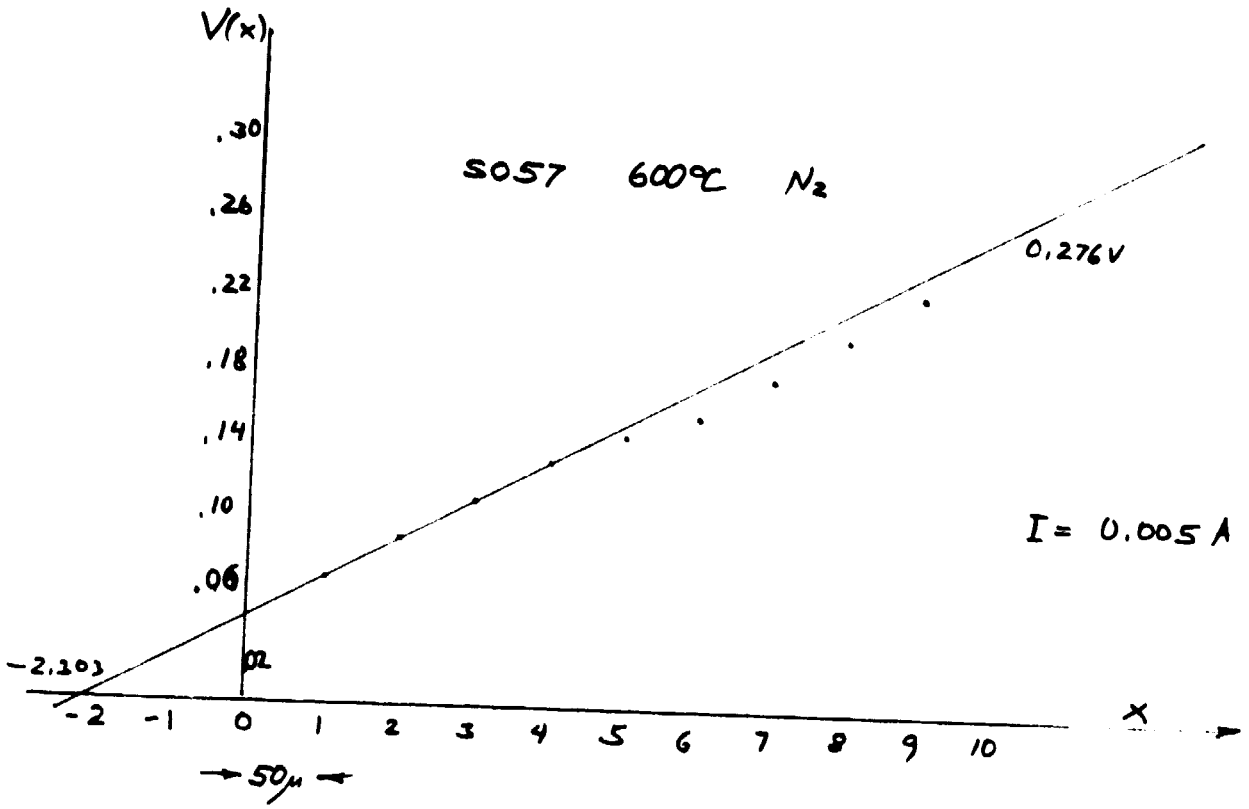

$$R_\square = \frac{0.276}{.005} \cdot 0.1 = 5.4\ \Omega/\square$$

$$R_c = 7.2 \cdot 10^{-4}\ \Omega cm^2$$

Figure 47

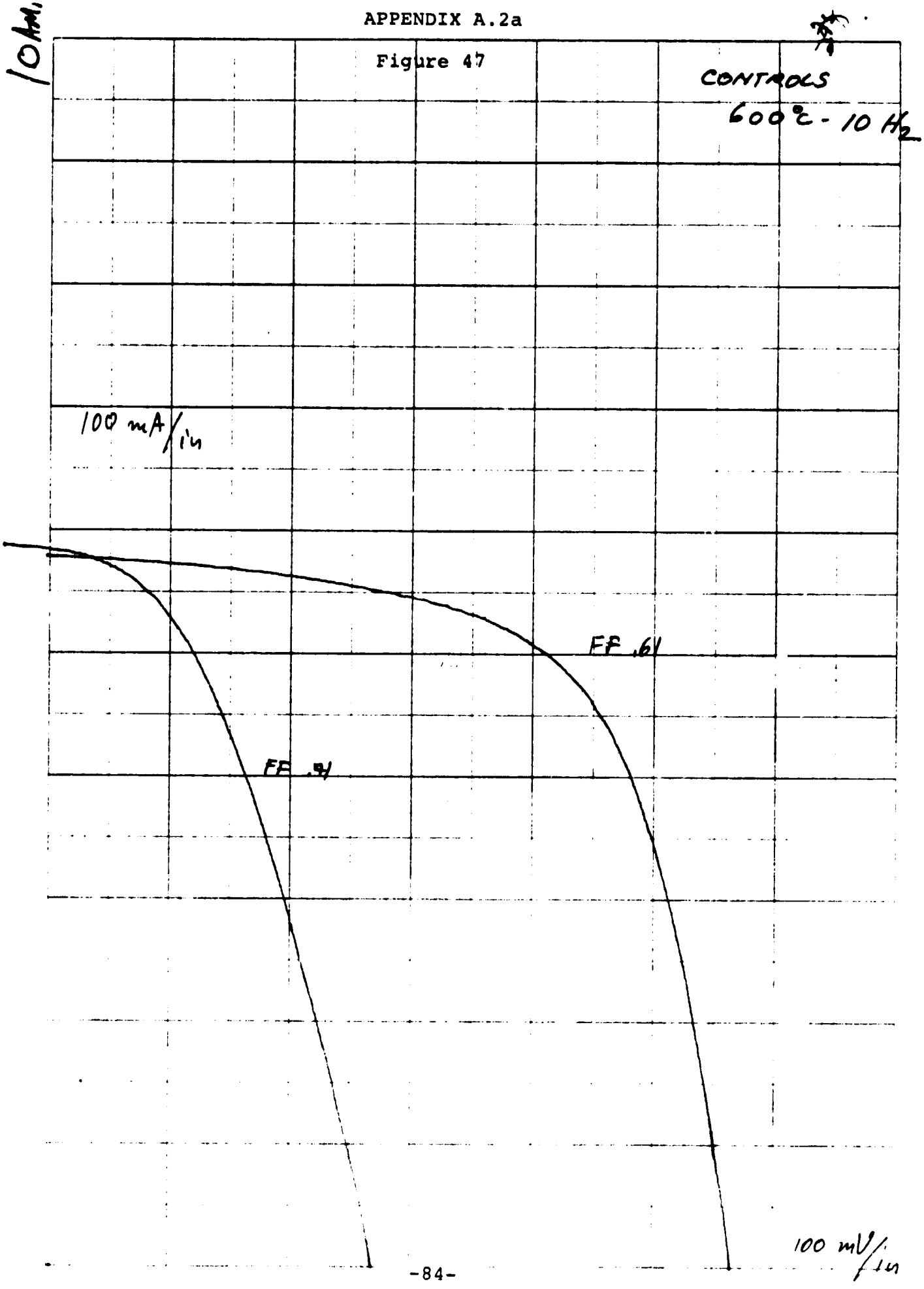

Figure 48

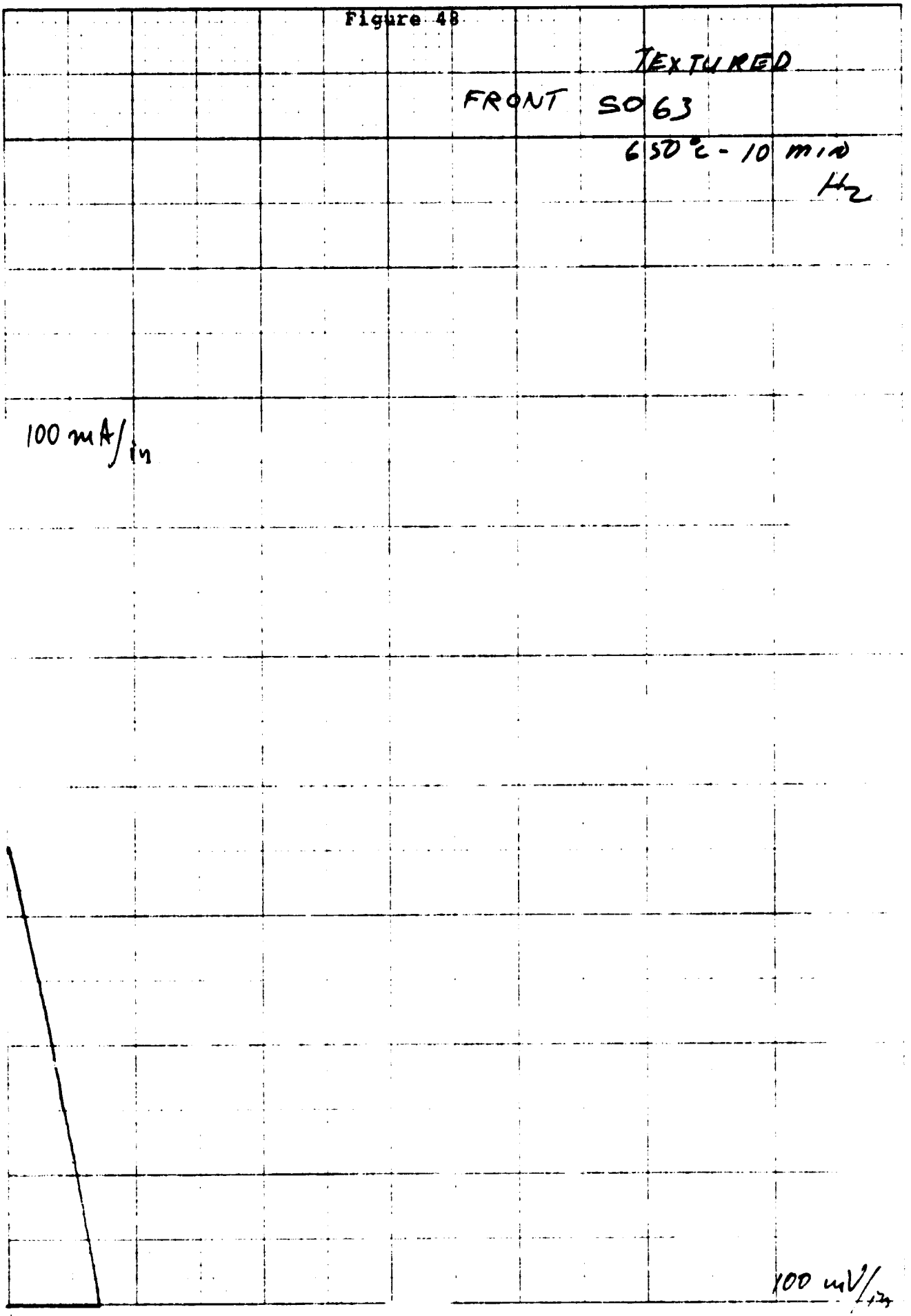

Figure 49

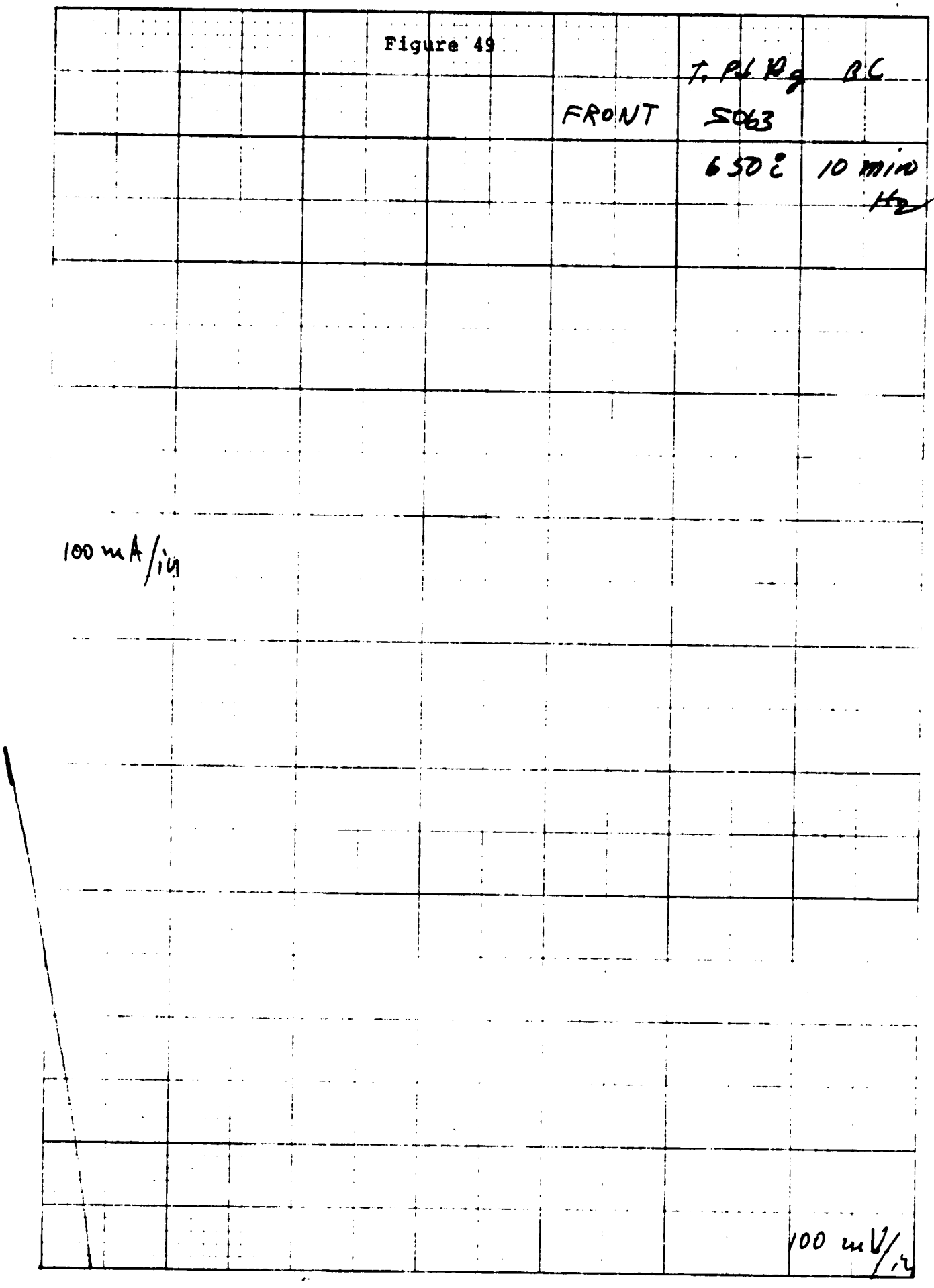

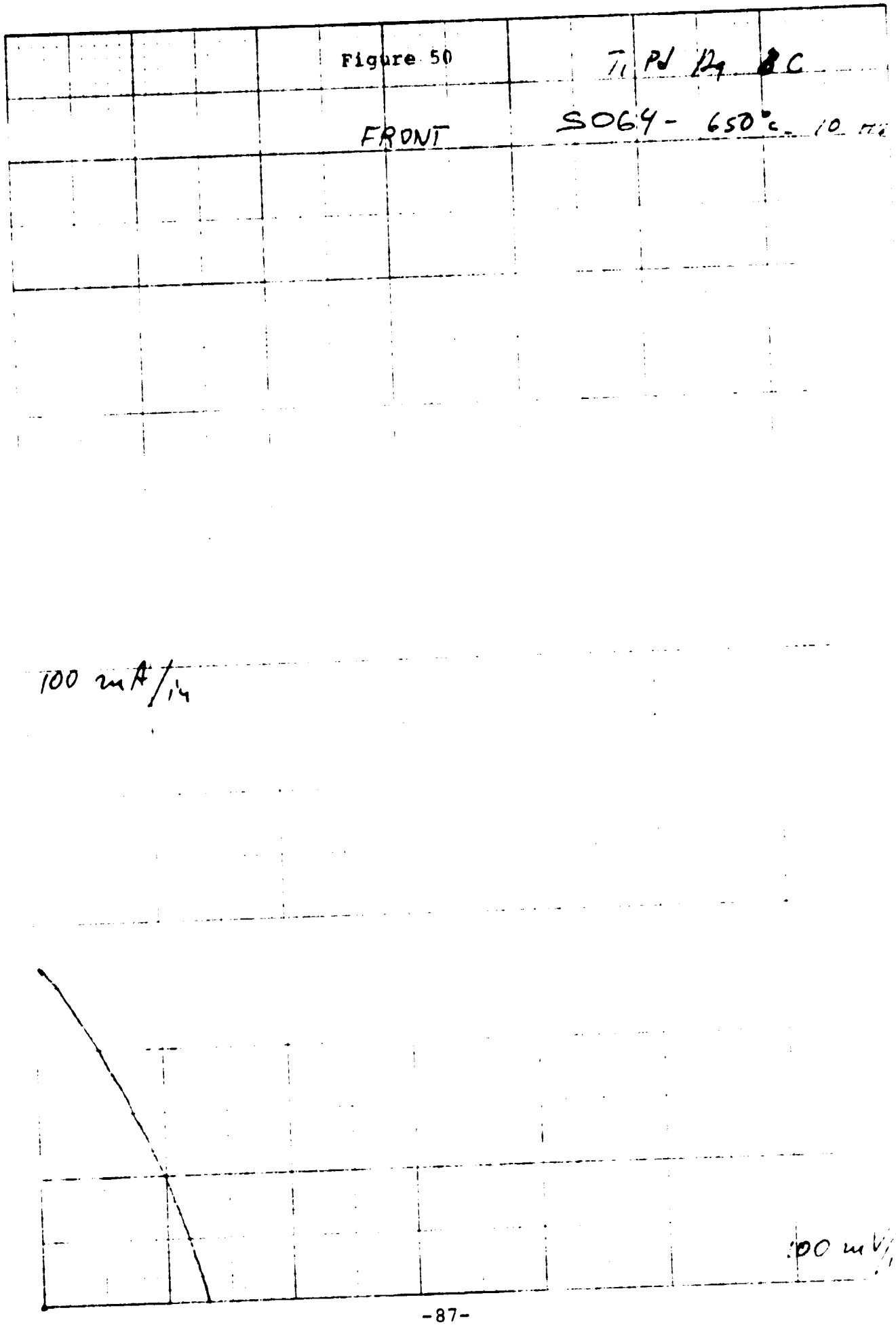
Figure 50
Ti Pd Ag C
FRONT
S064 - 650°C 10 Hz
100 mA/in
100 mV/in

Figure 51

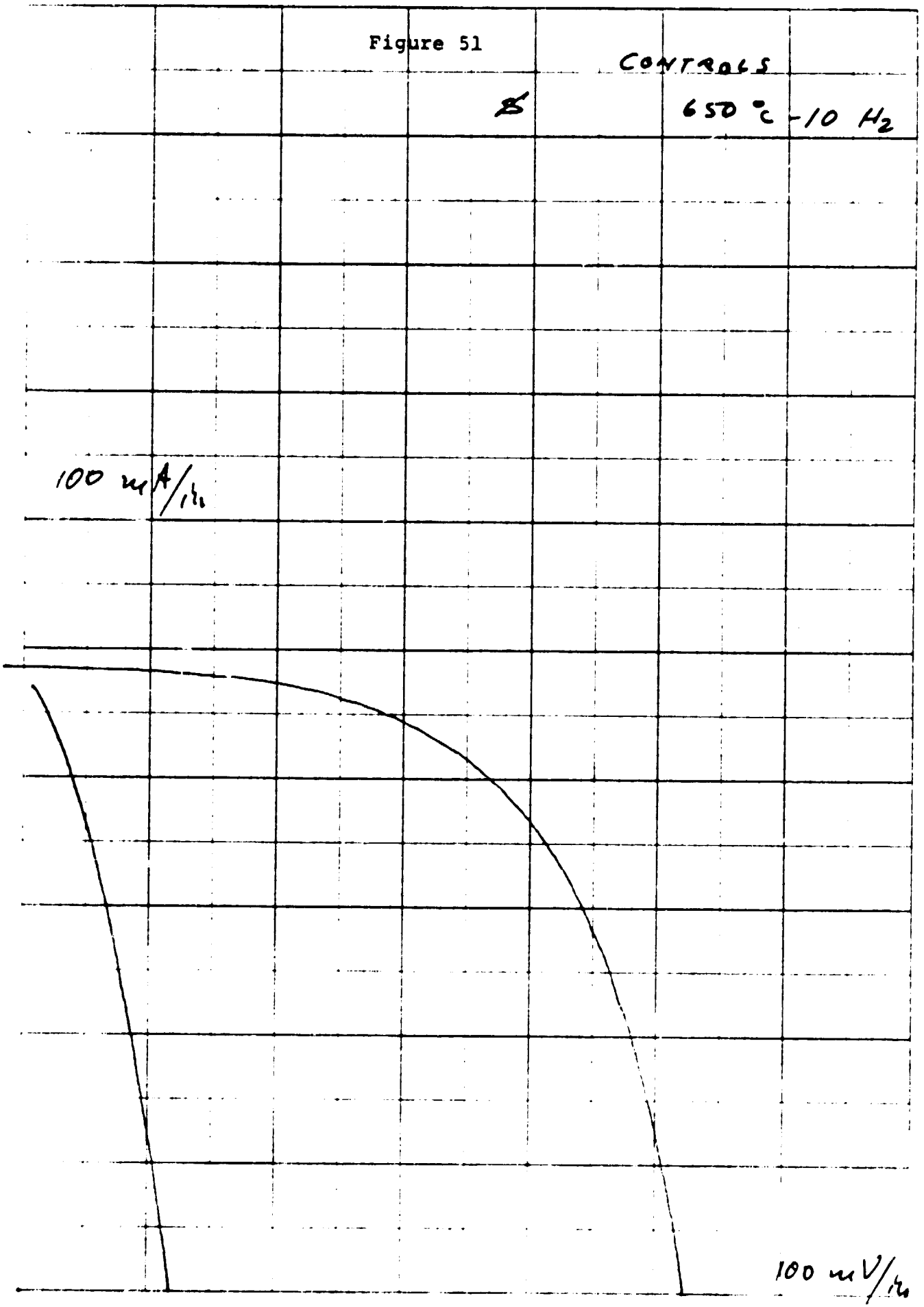

Figure 52

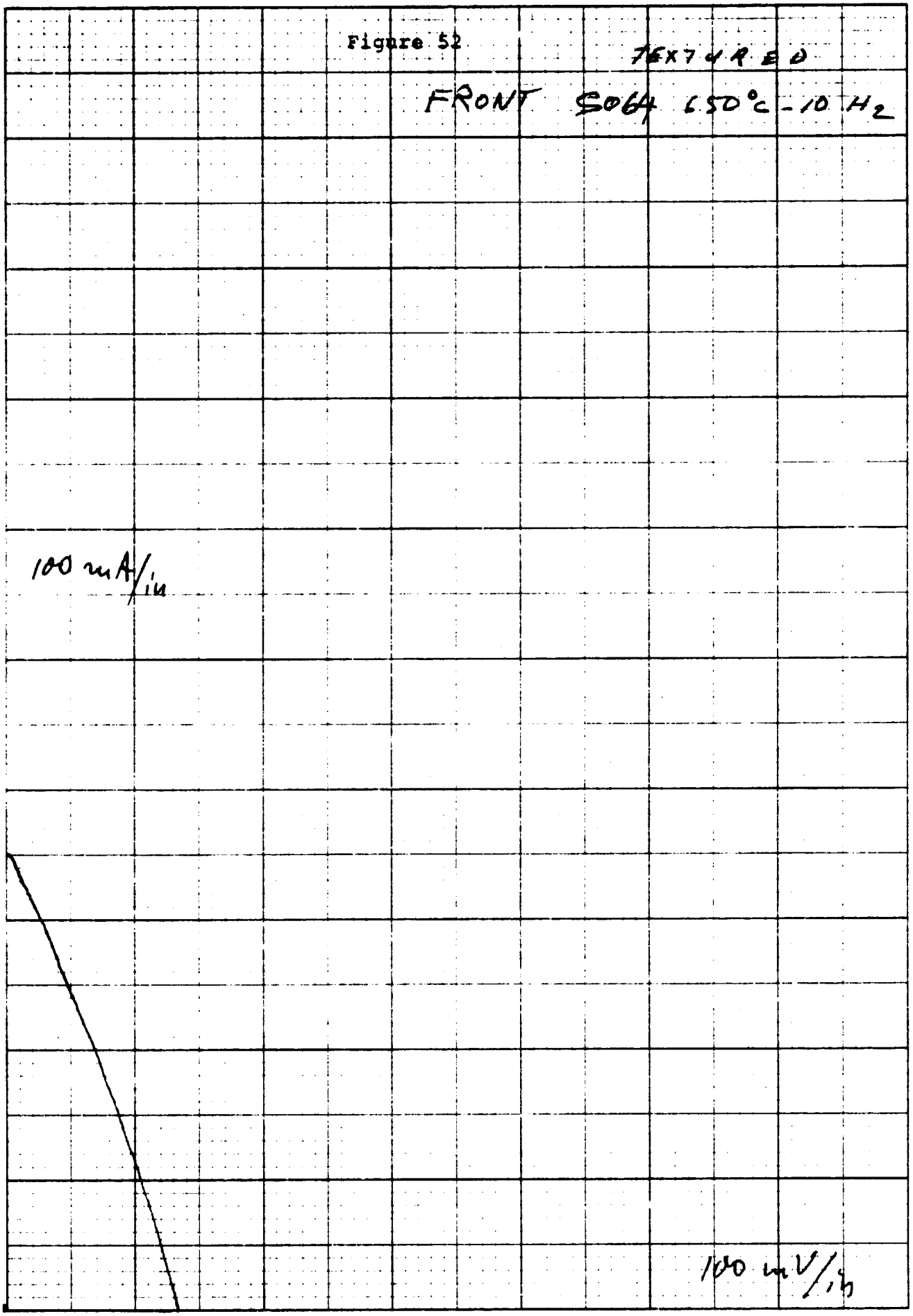

Figure 53

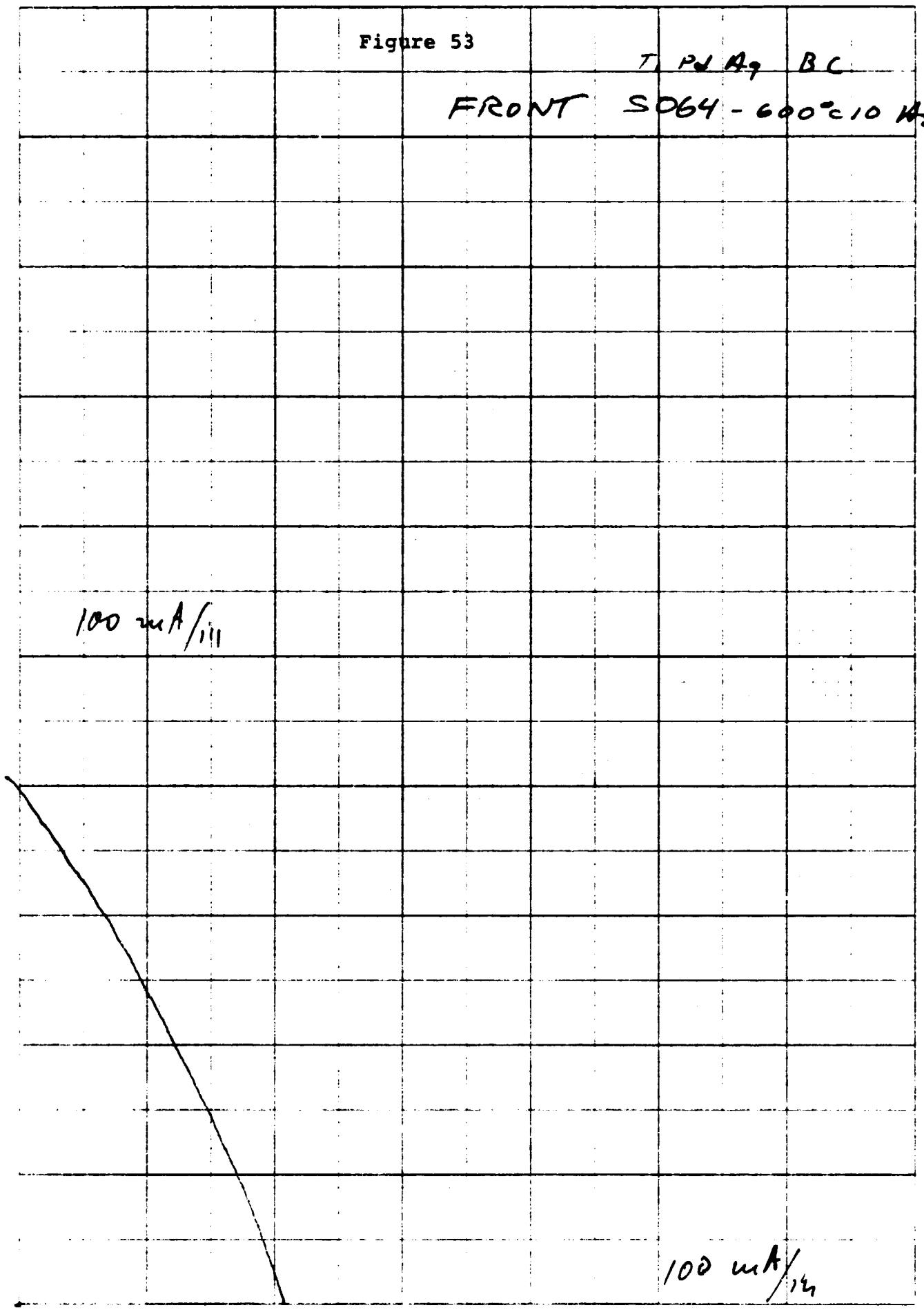

Figure 54

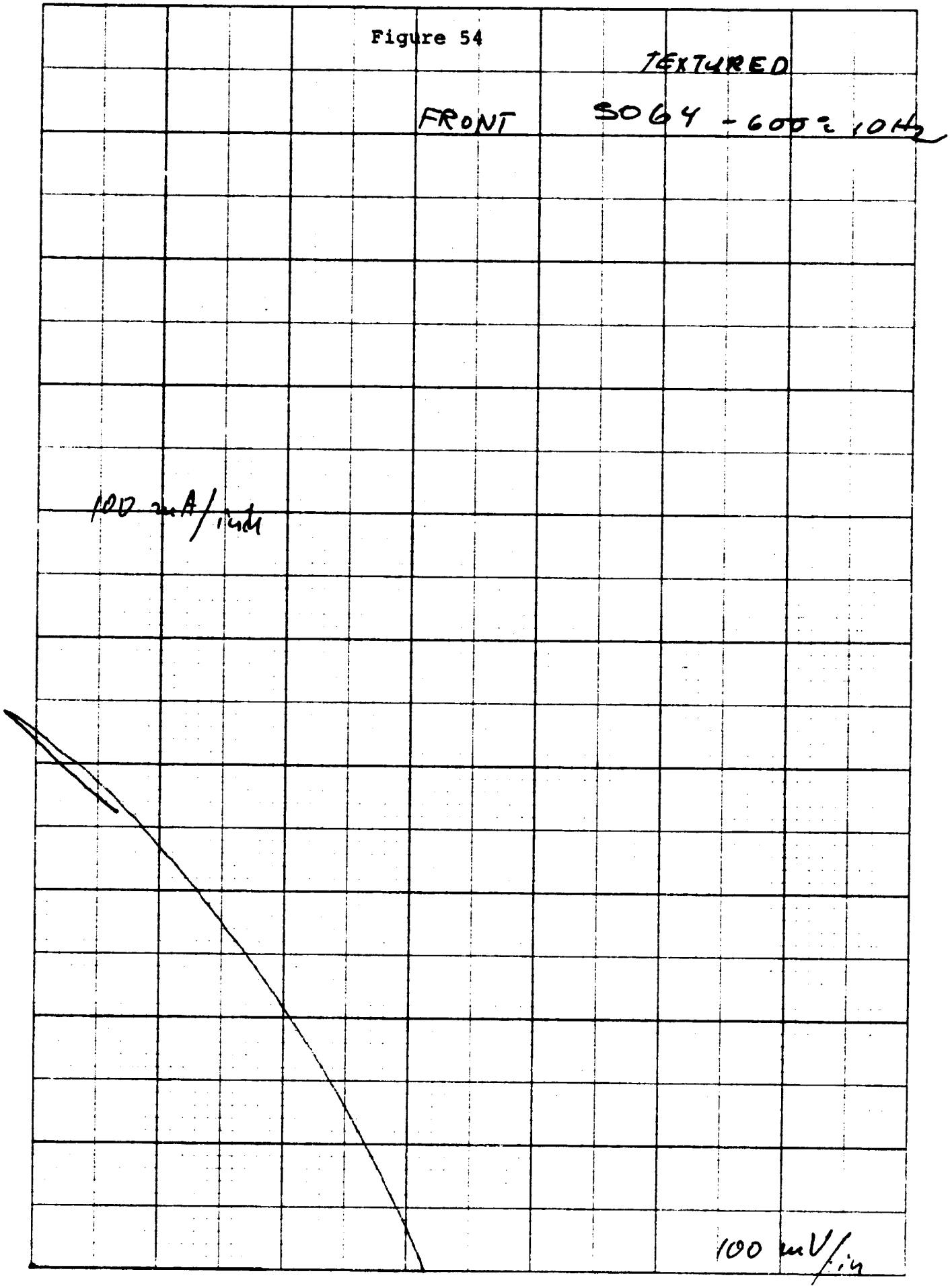

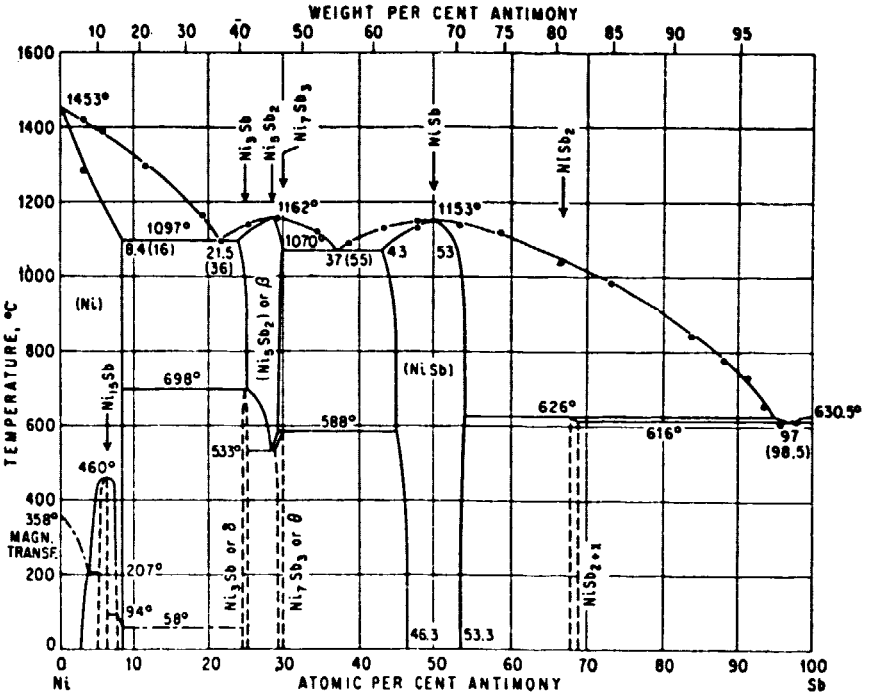

Fig. 55 Equilibrium Phase Diagram of Nickel-Antimony System.

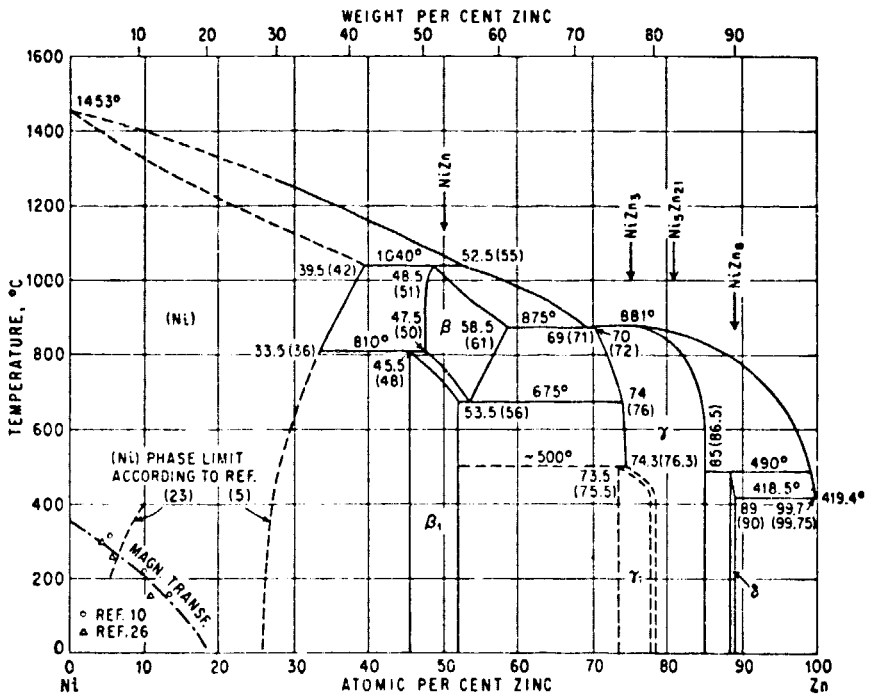

Fig. 56 Equilibrium Phase Diagram of Nickel-Zinc

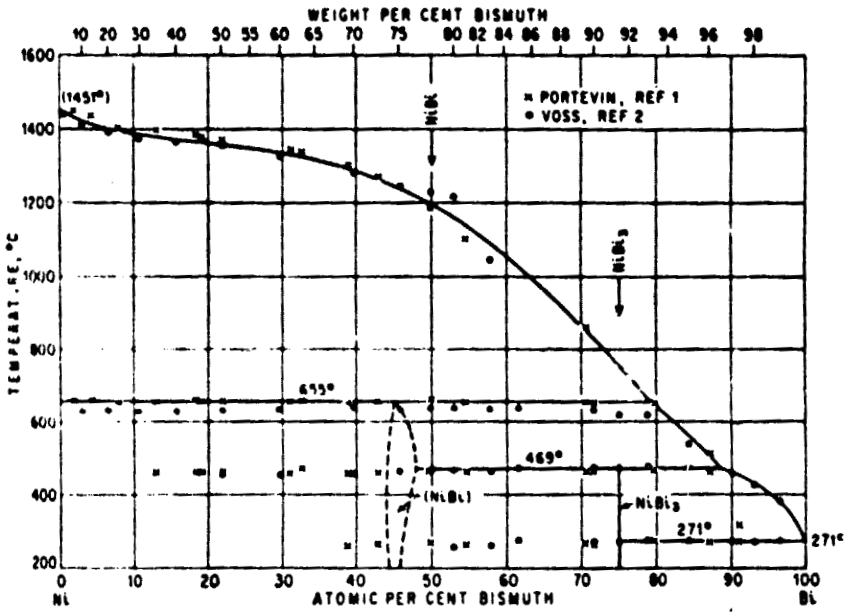

Fig. 57 Equilibrium Phase Diagram of Nickel-Bismuth.

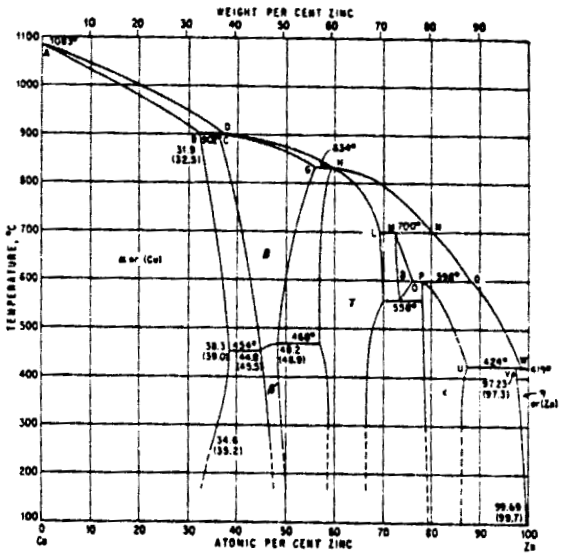

Fig. 58 Equilibrium Phase Diagram of Copper-Zinc.

A.3c

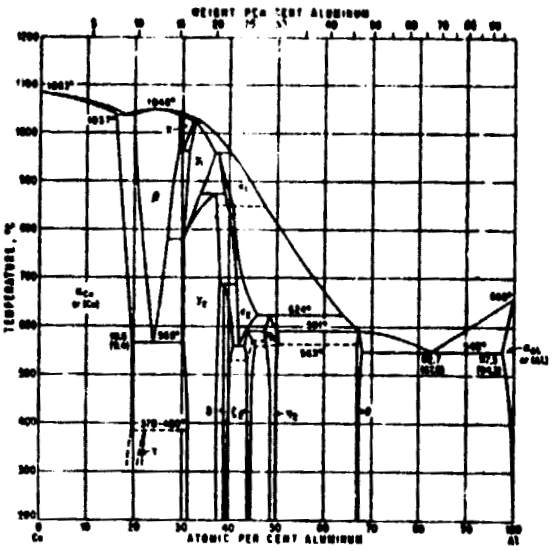

Fig. 59 Equilibrium Phase Diagram of Copper-Aluminum System.

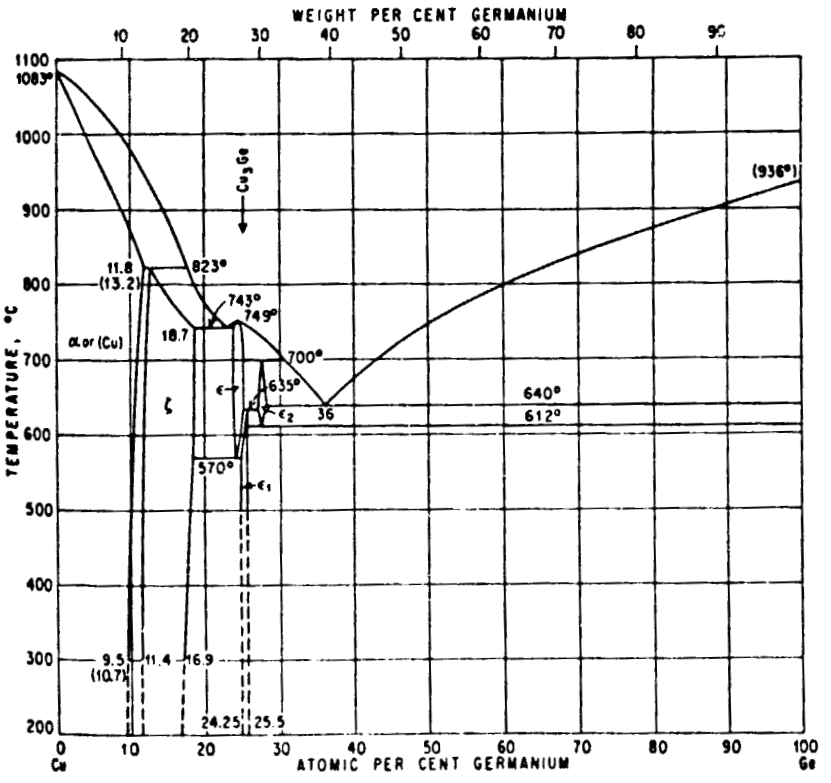

Fig. 60 Equilibrium Phase Diagram of Copper-Germanium System.

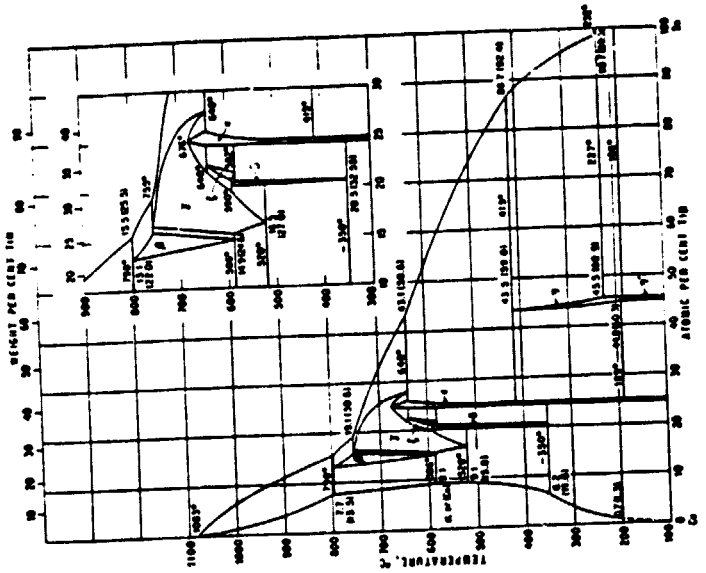

Fig. 62 Equilibrium Phase Diagram of Copper-Tin System.

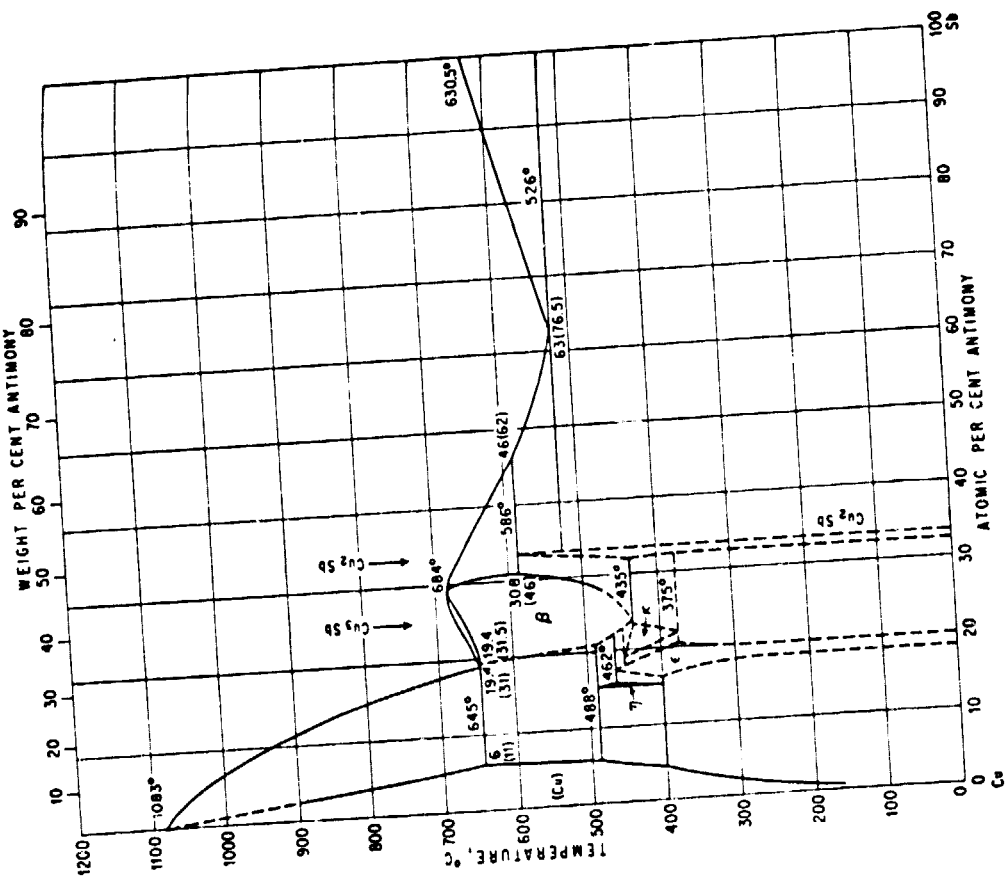

Fig. 61 Equilibrium Phase Diagram of Copper-Antimony System.

APPENDIX A.4a

650°C

Figure 63

AM 1 28°C

0.1 A/inch

650°C

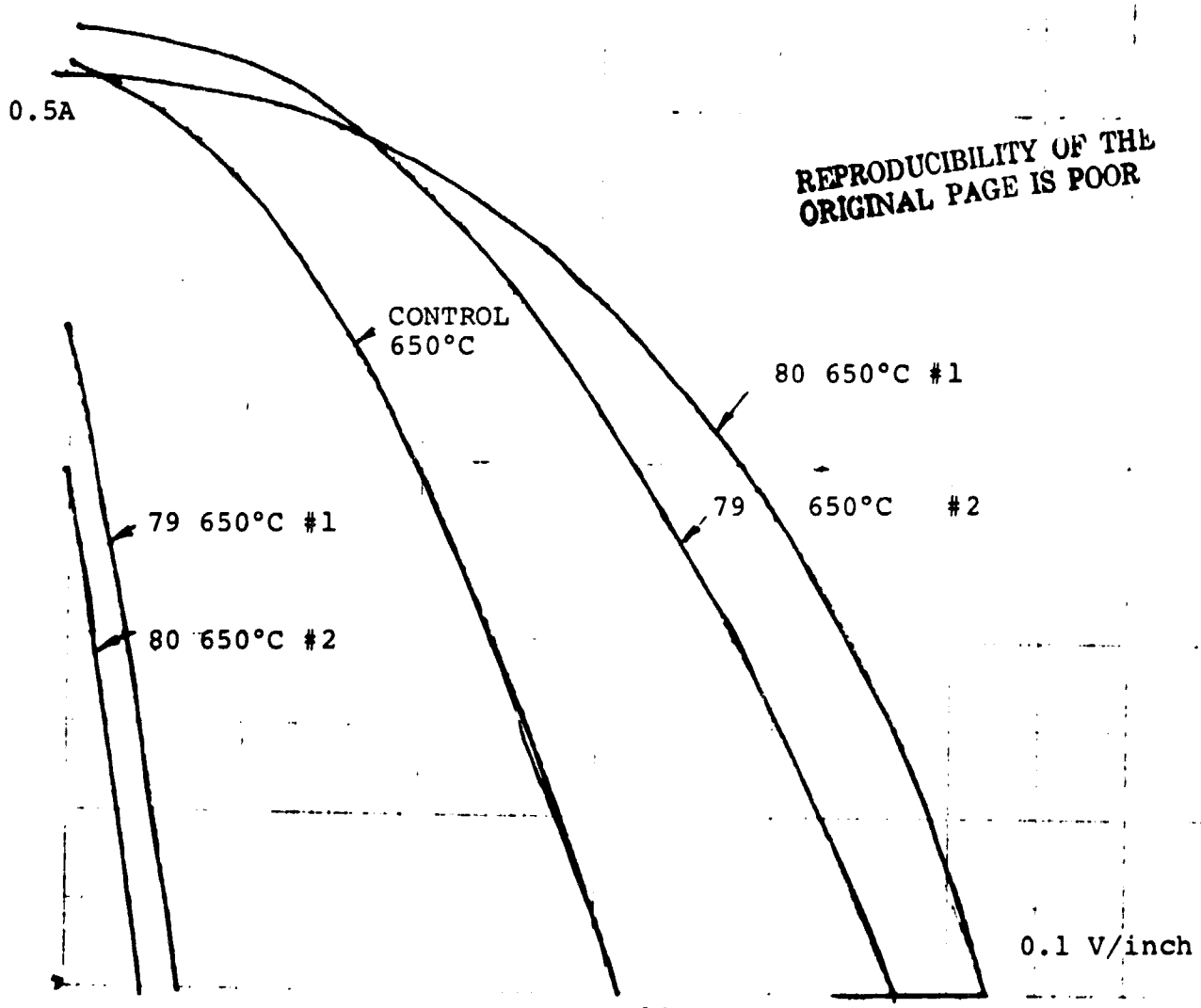

Figure 64

1/9/79

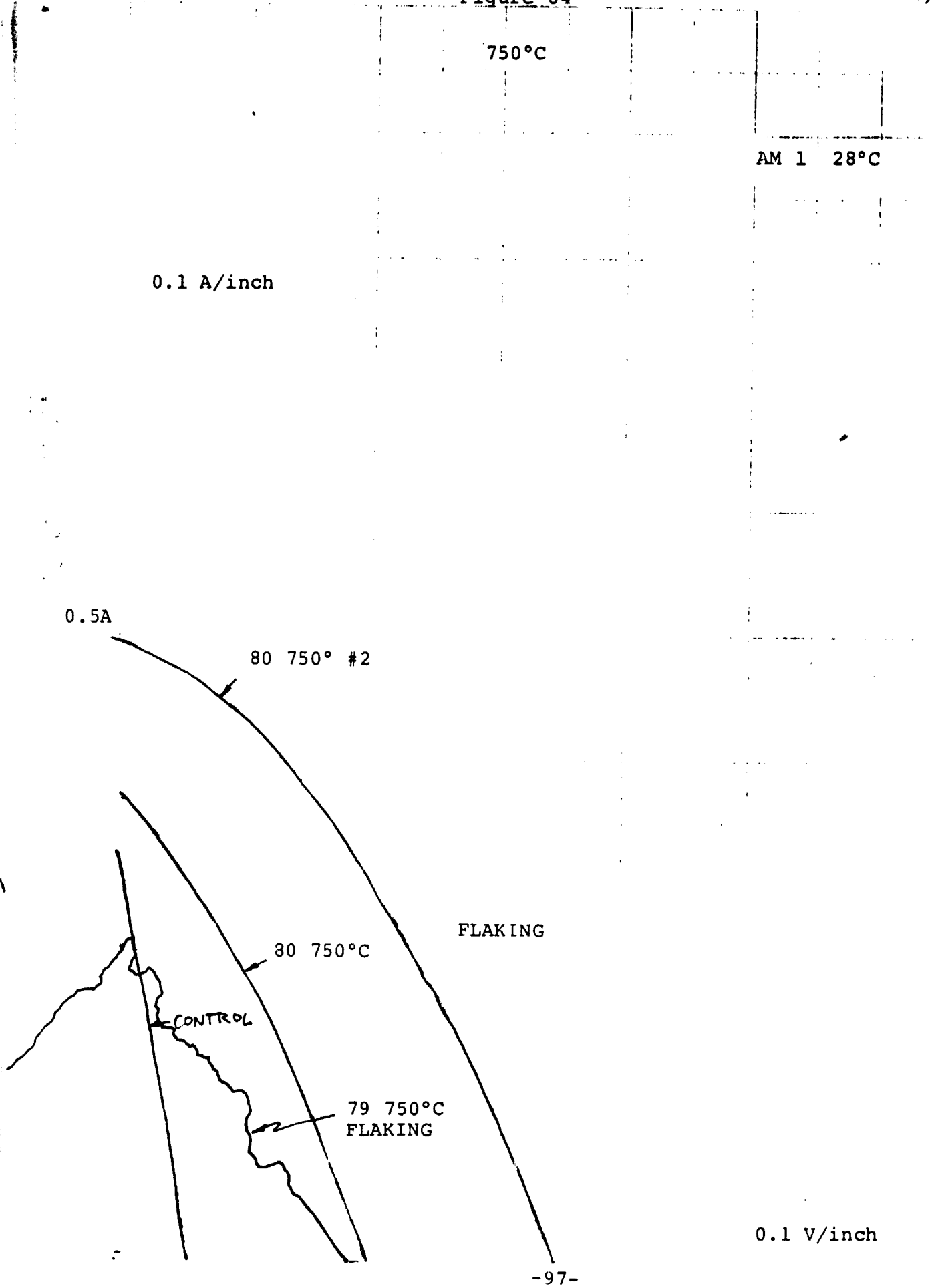

APPENDIX A.5

Figure 65

FURNACE TEMPERATURE PROFILE

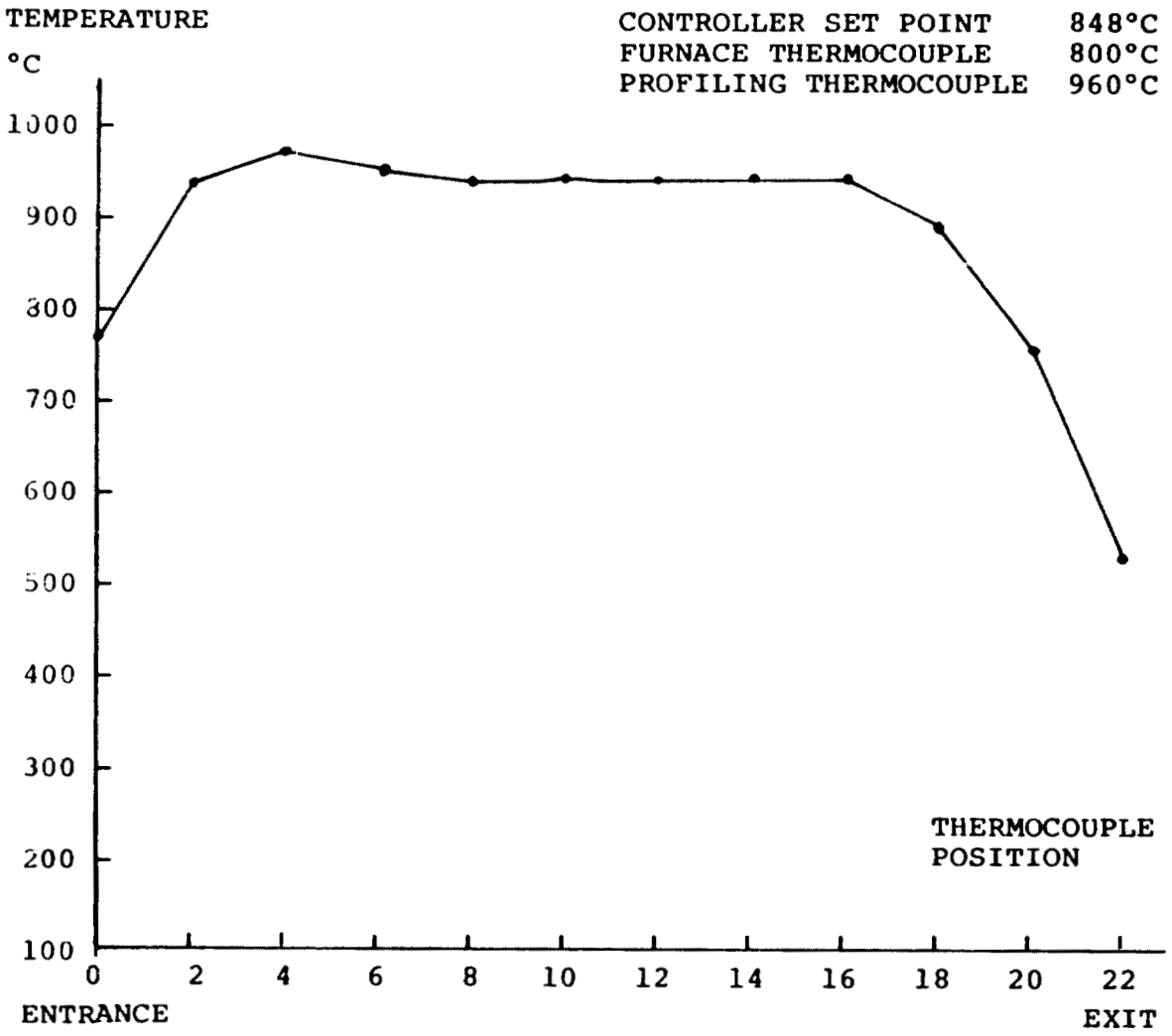

20.0 REFERENCES

1. A. Uhlir Jr., Bell Syst. Techn. Journ. 34, 105 (Jan 1955)

2. H.J. Hovel, Semiconductors and Semimetals, R.K. Willardson & A.L. Beer, Editors, Vol. II, p. 64, Academic Press (1975)

3. L.D. Swanson and L.W. Schmidt, Hoffman Semiconductor Division Publication (1960)

4. Hower, Hooper, Cairns, Fairman and Themore in Semiconductors and Semimetals, Volume 7 Part A, p. 178-183, Academic Press (1971)

5. C.A. Mead and W.G. Spitzer, Phys. Rev. 134, A 713 (May 1964)

6. B. Schwartz, Ohmic Contacts to Semiconductors, Ed. The Electrochemical Soc., p. 31, 69, 159 (1969)

7. B. Ross Final Report Automated Array Assembly Task DOE/JPL 955164-79/7 p. 38 (Apr 1979)

8. B. Ross Final Report Automated Array Assembly Task DOE/JPL 955164-79/7 p. 36 (Apr 1979)

9. M. Hansen and K. Anderko "Constitution of Binary Alloys", 2nd Edition McGraw-Hill, New York, N.Y. (1958)

10. C.B. Collins and R.O. Carlson, Phys. Rev. 108, 1409 (1957)

11. B. Ross and J.R. Madigan, Phys. Rev. 108, 1428 (1957)

12. R.H. Hopkins, J.R. Davis, P.D. Blais, A. Rohatgi, P. Rai-Choudhury, M.H. Hanes and J.R. McCormick, Quarterly Report #9, Silicon Materials Task DOE/JPL 954431-78/1, p. 46 (1978)

13. W.C. Dash, J. Appl Phys. 37, 1193 (1956)